Multi-objective Bi-level Programs for Optimal Microgrid Planning Considering Actual BESS Lifetime Based on WGAN-GP and Info-Gap Decision Theory

Hualong Liu, Wenyuan Tang

Department of Electrical and Computer Engineering, North Carolina State University, Raleigh, NC 27695, USA

Abstract

With the rapid development of society and economy, random and intermittent renewable energy such as wind and photovoltaic (PV) generation is connected to the grid on a large scale. At the same time, forecasts of renewable energy output and loads are imprecise. These factors together lead to the uncertainty of power systems increasingly showing the characteristics of Knightian uncertainty, which makes the optimal microgrid planning and operation very challenging. Firstly, to overcome the shortcoming of the Monte Carlo method and the Latin hypercube method that require prior knowledge of the probability distributions of renewables and loads, this paper proposes a typical scenario generation methodology for renewables and loads based on Wasserstein generative adversarial networks with gradient penalty (WGAN-GP) and K-medoids. Secondly, optimal multi-objective bi-level microgrid planning models considering the actual battery energy storage system (BESS) lifetime based on WGAN-GP and info-gap decision theory under opportuneness and robustness strategies are established in this paper to effectively resolve the Knightian uncertainty of optimal microgrid planning and operation caused by the uncertain nature of wind, PV generation, and loads. Then, the multi-objective bi-level models are converted into multi-objective single level models. The Pareto-optimal front of these multi-objective problems are obtained by the ϵ-constraint method, and the compromised solution of the Pareto-optimal set is determined by fuzzy decision making. Finally, the proposed models are analyzed on the Banshee microgrid and verified by the Monte Carlo simulation. A bunch of results based on cases studies are obtained. For example, under the opportuneness strategy, when the opportunistic level factor equals 0.20 and the radii of the uncertainties of wind, PV generation, and loads are 0.0625, 0, and 0.2298, respectively, the planning cost of the microgrid does not exceed \$2048k. This case reduces the cost by 20% compared to deterministic planning. All results of case studies prove the reliability, feasibility, and effectiveness of the proposed models.

Keywords: Distributed energy resources (DERs), energy storage, microgrid, Wasserstein generative adversarial networks with gradient penalty (WGAN-GP), optimal planning and operation, info-gap decision theory, multi-objective, renewable energy, uncertainty.

1. Introduction

1.1. Research motivation

Because of growing concerns over greenhouse gas emissions by conventional energy generation sources, microgrids are becoming a viable solution for integrating distributed energy resources (DERs) to reduce environmental pollution. In general, DERs include renewable energy sources (RESs), energy storage systems (ESSs), dispatchable fuel-generators (DFGs), etc [1]. The battery energy storage system (BESS) is a kind of ESS.

There have been several researches on microgrid planning. However, most of them are based on single-bus approaches, that is, they do not consider dynamic constraints such as power flow. The single-bus model cannot perform the optimal placement of DERs inherently, which is obviously unreasonable. Furthermore, many studies on microgrid planning regard the BESS lifetime as a fixed value, which is obviously unrealistic, because the frequent use of the BESS makes its actual service lifetime lower than the nominal lifetime. Hence, our models not only consider dynamic constraints such as power flow, but also consider the actual BESS lifetime based on the rain-flow counting algorithm.

Traditional scenario generation methods such as the Monte Carlo method and the Latin hypercube method need to assume in advance that the data obey specific probability distributions in order to generate scenarios. However, it is difficult to obtain the probability distributions accurately in actual engineering practice. In addition, the modeling process of the Monte Carlo method and the Latin hypercube method is tedious. These drawbacks of the Monte Carlo method and the Latin hypercube method may produce large errors in the process of parameter fitting and generate poor-quality scenarios. Consequently, this paper adopts the Wasserstein generative adversarial networks with gradient penalty (WGAN-GP) rather than the traditional scenario generation methods to generate scenarios. WGAN-GP does not need to assume the data distribution in advance, and avoids the problem that the assumed distribution in traditional methods is different from the actual distribution, which leads to unreasonable scenario generation.

Wind and photovoltaic (PV) generation are connected to the grid on a large scale because they are environmentally friendly, low-cost, and renewable. However, in the context of a competitive power market, microgrid planning decision-makers may not have access to complete wind and PV generation output and load data due to privacy concerns of generation enterprises. Furthermore, wind and PV generation have strong intermittence and randomness, load management makes load side structure change, and the load is affected by the subjectivity of electricity consumption, etc. Moreover, due to the limitations of forecasting technology and cognitive ability, these factors make it difficult to accurately obtain the actual wind, PV generation, and loads. The above factors together make the uncertainty in the power system increasingly exhibit characteristics of Knightian uncertainty. The uncertainty seriously affects the design, security, stability, and economic operation of the microgrid, which makes the planning and operation of the microgrid a very challenging job. If uncertainties are not properly addressed, they can lead to serious planning and scheduling issues, such as inadequate unit climbing capacity, insufficient rotation reserves, transmission congestion, and demand disruptions. In this context, it is of great significance to study the optimal planning and operation of microgrids that take into account the uncertainties pertaining to renewables and loads, yet underestimating or exaggerating the impact of uncertainty in the optimal planning and operation of microgrids can jeopardize the reliability and cost-effectiveness of microgrids. Therefore, uncertainty must be seriously considered in the optimal planning and operation of microgrids.

At present, there are four main modeling methods of uncertainty in power systems, namely, fuzzy programming [2, 3, 4, 5, 6, 7], stochastic programming [8, 9, 10, 11, 12, 13, 14, 15, 16], interval methods [17, 18, 19, 20, 21, 22, 23], and robust optimization [24, 25, 26, 27, 28, 29, 30, 31]. The key to modeling based on fuzzy optimization lies in the selection of membership functions; on this basis, the necessary judgment conditions are added to form the power system uncertainty model. Stochastic programming holds that the uncertainty of a system can be described by probability distribution functions. Stochastic programming requires knowing the probability distributions of the parameters. Scenario-based stochastic programming involves a large number of scenarios and a large amount of calculation. Although the probability distributions of uncertain variables are not required for robust optimization, the exact set of uncertainties in robust optimization can lead to overly conservative solutions, which can cause the economy

of the system to decline. These traditional methods need to have sufficient knowledge of uncertainty in order to obtain membership functions, probability distributions, specific interval ranges, or bounded uncertainty sets. However, such prior information is difficult to obtain in practical engineering applications, especially under power systems' increasingly displaying Knightian uncertainty. Moreover, we used to think that uncertainty was bad; however, not necessarily, in some cases, uncertainty can be beneficial.

Compared with stochastic, fuzzy programming, robust optimization, and interval methods, info-gap decision theory [32] examines the characteristics of uncertainty from the perspective of non-probability. Info-gap theory pays attention to the gap between known information and unknown information, and the modeling is simple. It has a small demand for uncertain information and does not need probability distributions, membership functions, uncertainty boundaries, or uncertain intervals. It can guarantee the economy of the system while ensuring the robustness of the system. It is insensitive to parameter perturbations. It can deal not only with robustness model, but also with chance model. It has stronger applicability to Knightian uncertainty in modern power systems. Info-gap theory is unique in that it expresses the idea that uncertainty can be both harmful and beneficial, and quantifies both aspects of uncertainty. These advantages of info-gap theory stimulate the authors to explore its use in dealing with uncertainties in the planning and operation of microgrids.

1.2. Literature review

1.2.1. Deterministic planning

Reference [33] discussed the economic emission load dispatch-based scheduling of DERs for proper energy management planning. Reference [34] proposed a model for calculating the optimal ESS size of a microgrid considering the reliability criterion. Reference [35] developed the operation and design optimization model of microgrids with renewables. Reference [36] presented the operational strategy optimization in an optimal sized smart microgrid, where energy management in microgrids is addressed taking into consideration economic efficiency, environmental restrictions, and reliability improvement. In [37], the optimal planning of a microgrid including demand response and intermittent RESs was proposed, which investigated the suitability of a novel active controller applied to heating/cooling systems in a microgrid with high penetration of renewables. Reference [38] presented a hybrid combined cooling, heating, and power (CCHP) system integrated with compressed air energy storage (CAES). Reference [39] discussed the optimal operational planning of scalable DC microgrid. Reference [40] presented AC versus DC microgrid planning.

The microgrid planning problem is typically formulated as a mixed integer programming problem, which is an NP-hard problem. Researchers have used different mathematical methods to model and approach the problem of optimal microgrid planning and operation. References [41, 42, 43] applied the mixed integer linear programming (MILP) to the planning problem of microgrids. Particle swarm optimization was employed for the redundant building cooling heating and power system in [44] and for the hybrid micro-grid system in [45]. Reference [46] used genetic algorithms to design and control PV-diesel systems. A two-stage optimal planning and design method was adopted for the CCHP microgrid system in [47]. Multi-objective formulations were utilized in [48, 49, 50, 51]. Reference [52] applied a duality-based approach to short-term operation scheduling in renewable-powered microgrids. Reference [53] established a two-stage full-data processing method for microgrid planning with high penetration of renewables. A mixed integer nonlinear model was developed in [54], in which a deterministic branch-and-bound nonlinear solver was utilized. A bi-level program for the planning of an islanded microgrid including CAES was presented in [55]. Two constraint-based iterative search algorithms were proposed for the optimal sizing of wind turbines (WTs), solar PV panels and BESSs in a grid-connected microgrid in [56]. Reference [57] proposed a cost-effective two-stage

optimization model for microgrid planning and scheduling with CAES and preventive maintenance.

1.2.2. Fuzzy programming

In order to deal with the risks brought by uncertainty to microgrid planning, there have been a large number of relevant studies, which mainly focus on microgrid planning and operation based on fuzzy programming, stochastic programming, interval methods, and robust optimization. Reference [2] discussed the applications of fuzzy logic in planning of microgrids. In Reference [3], a multi-objective fuzzy optimization model was established for electricity generation and consumption management in a microgrid. Reference [4] proposed a methodology based on fuzzy interval models for microgrid planning which includes the effect of the uncertainties of renewables explicitly. An economic dispatch algorithm with fuzzy wind constraints and attitudes of dispatchers was described in Reference [5]. A fuzzy optimization approach for solving the generation scheduling problem with wind and solar energy systems was presented in Reference [6]. An energy operation model for optimizing operation costs of a non-isolated microgrid was proposed in Reference [7]. Different possible uncertainties associated with different elements of the microgrid like the output of renewable sources, the maximum capacity of batteries, the maximum capacity of distributed line, and hourly demand are considered in this model. Fuzzy sets are used to model these uncertainties, and a three stage optimization method is applied to find the optimal scheduling of the microgrid under the uncertainties.

1.2.3. Stochastic programming

In Reference [8], a predictive control approach to integrated energy management based on the stochastic model was presented for a microgrid with renewables. The uncertainties of load demand, wind, and PV generation in the microgrid as well as the electricity prices are modeled by typical scenarios. A two-stage energy management scheme of hybrid AC/DC microgrids was proposed based on stochastic programming in [9]. This scheme uses scenario-based stochastic programming and considers frequency security constraints. A two-stage stochastic p-robust optimal energy trading management method for microgrid operation was presented in [10]. This method takes into account uncertainty and hybrid demand response, and assumes that the probability density functions of renewable generation are known. In Reference [11], a two-stage stochastic programming formulation was proposed. The conventional generation schedules and adjustable load set points are first-stage decisions. However, second-stage decisions include energy transactions with the main grid and real time load adjustments. Multi-objective stochastic programming energy management in microgrids was developed in Reference [12]. Uncertainties of wind speed, solar radiation, and electrical-thermal loads are investigated, and a multi-objective stochastic MILP is solved in the first stage. Then, in the second stage, the effects of fuel cost uncertainty on generation units and objective functions are studied. Two-stage stochastic programming formulation for the optimal design and operation of the multi-microgrid system using data-based modeling of renewables was presented in Reference [13]. A multi-objective stochastic optimization methodology for planning a multi-energy microgrid considering unscheduled islanded operation was established in Reference [14]. In this reference, the model of the uncertain islanded mode is developed using four correlated random variables, and the scenario tree is employed for islanded scenario generation. Cao *et al.* [1] presented a chance constrained information gap decision model for multi-period microgrid expansion planning. A chance-constrained optimization problem was formulated for the optimal scheduling of mirogrids in [58]. A scenario-based stochastic programming framework for multi-objective optimal microgrid operation was developed in Reference [59]. In the framework, the uncertainties related to the forecasted values for load demand, wind, PV units, and market prices are modeled by scenario-based stochastic programming. A two-stage stochastic programming method to incorporate the various possible scenarios for RESs and costs in the microgrid planning was

introduced in Reference [60]. Hajipour *et al.* [61] presented the stochastic capacity expansion planning of remote microgrids with wind farms and energy storage. A stochastic programming framework for day-ahead scheduling of microgrid energy storage systems using multi-objective optimization was proposed in Reference [15]. To properly handle the uncertainties, stochastic models associated with renewables and loads are developed in the multi-objective scheduling framework and they are formulated as MILP problems. Reference [16] presented a stochastic multi-objective optimal energy management algorithm of grid-connected unbalanced microgrids with renewables and plug-in electric vehicles. Uncertainties are considered by employing the roulette wheel mechanism for generating scenarios. A hybrid stochastic/robust-based multi-period investment planning model for isolated microgrids was presented in [62].

1.2.4. Interval methods

Optimal planning of multi-energy microgrids with uncertain renewables and demand based on the interval method was proposed in [17]. The uncertainties of RESs and demand are described as intervals, and the corresponding uncertainty constraints could be converted to deterministic ones. Interval optimization was applied to the coordination of demand response and BESSs in a microgrid in [18]. Multi-objective optimal dispatch of microgrids under uncertainties via interval optimization was developed in [19]. Uncertain power output of wind and PV generation in a microgrid are presented as interval variables. A multi-objective interval optimization dispatch model for microgrids via deep reinforcement learning was formulated in [20], where the uncertain power output of wind and PV generation is represented by interval variables. A hybrid stochastic-interval operation algorithm for multi-energy microgrids to account for uncertainties in decisions of operational strategies was proposed in [21]. Reference [22] developed an interval-based privacy-aware optimization framework for electricity price setting in isolated microgrid clusters, in which the uncertain nature of renewable generation and demand is accommodated using interval notation and equivalent scenarios. Reference [23] proposed a stochastic-based resource expansion planning scheme for a grid-connected microgrid using interval optimization, where interval linear programming is applied for modelling inherent stochastic nature of renewables.

1.2.5. Robust optimization

A robust offering algorithm for wind producers considering uncertainties of demand response and wind generation was proposed in [24]. This is a risk-constrained decision-making method. A robust framework for the day-ahead energy operation of a residential microgrid comprising interconnected smart users under uncertainties of demand and renewable power generation was presented in [25]. Expansion planning for a distribution network considering the uncertainties of wind generation and loads was handled by adaptive robust optimization based on polyhedral uncertainty sets [26]. A scenario-based robust energy management scheme of a microgrid with uncertain renewables and loads was described in [27], which considers the worst-case amount of renewables and loads. Reference [63] proposed a robust optimization method for optimal DG placement in microgrids considering the uncertain nature of renewables and loads. This model is converted into a two-stage robust optimization problem, and a column and constraint generation method is employed to tackle it. A distributionally robust optimization model for real-time power scheduling of distribution networks was presented in [28]. This model can be reshaped into a semidefinite programming problem and handled by a constraint generation algorithm. A two-stage robust optimization method for spatially-temporally correlated data centers was established in [29]. The boundaries of the uncertainty sets are handled by a data-driven approach. A two-stage robust reactive power optimization strategy in active distribution networks with wind generation was proposed in [64]. This model can give a robust optimal solution and coordinate the discrete and continuous reactive power compensators. An inexact two-stage stochastic robust programming was used to find the optimal planning and operation

of residential microgrids in [65]. A tri-level robust investment planning scheme of DERs in distribution networks was proposed in [66]. A point estimate-based stochastic robust scheduling model for electricity-gas combined systems with probabilistic wind generation was proposed, and the model was solved using iterative convex optimization in [31]. Reference [30] developed a tri-level robust planning-operation co-optimization scheme of distributed energy storage in distribution networks with high PV penetration. This reference analyzes the effect of different level uncertainties on the solutions of the planning problem. A robust optimization model for the microgrid planning problem with uncertain physical and financial information was presented in [67].

1.2.6. Info-gap decision theory

Info-gap decision theory has been applied to a certain extent to market bidding strategies [68, 69], reactive power planning [70], voltage management [71], optimal power flow [72], unit commitment [73, 74, 75], and energy scheduling [76, 77, 78, 79, 80, 81]. Reference [68] utilized info-gap decision gap to deal with the optimal bidding strategies for the day-ahead market. Reference [69] considered the uncertainty caused by wind generation based on info-gap decision theory, and developed a risk-based energy management scheme of renewable-based microgrids in the presence of peak load management. A reactive power planning scheme based on info-gap decision theory was developed in [70]. In this reference, info-gap decision theory is utilized to tackle the uncertainties of wind farms and loads. In [71], info-gap theory was used to deal with congestion and voltage management in the presence of the uncertainty of wind generation. References [72] and [73] applied info-gap decision theory to the optimal power flow and unit commitment problems of power systems considering wind generation uncertainty, respectively. Reference [74] applied info-gap decision theory to robust security-constrained unit commitment considering wind generation and electric vehicles. Reference [75] utilized info-gap decision theory to handle the uncertain nature of wind generation and evaluated the effect of electric vehicle parking lots on transmission-constrained unit commitment using a hybrid IGDT-stochastic approach. References [76] and [77] utilized info-gap theory to tackle the scheduling problems of concentrating solar power plants and wind producers, respectively. A risk-seeking economic dispatch method based on info-gap decision theory considering the uncertainties of wind generation was presented in [78]. A robust operation approach of integrated electricity and natural gas transmission networks was developed in [79], in which the uncertainty of load demand is considered. The uncertainties considered in this reference are photovoltaic generation and load demand. An optimal day-ahead scheduling approach of DERs using info-gap decision theory was presented in [80], where the uncertainties of PV generation and loads are examined. Risk-constrained self-scheduling schemes of generation companies based on info-gap decision theory were proposed in [81]. A complementarity approach of virtual power plants based on info-gap decision theory was developed in [82]. This approach can handle strategic decision making of price-maker virtual power plants considering demand flexibility. A charging optimization approach for electric vehicles considering demand response and multi-uncertainties based on Markov chain and info-gap decision theory was developed in [83]. This approach analyzes the impact of fluctuations in wind and PV generation on risk aversion decision makers using info-gap decision theory. Info-gap decision theory was employed to enhance the resilience of active distribution systems in [84]. Scheduling strategies of the integrated natural gas and power system with high wind generation were developed in [85, 86], in which info-gap decision theory is utilized to handle the uncertain nature of wind generation. A info-gap decision theory-based robustness assessment method for a power system with wind generation penetration considering rigorous security constraints was presented in [87].

However, the application of info-gap theory in optimal microgrid planning and operation remains to be studied. In addition, there are some problems such as incomplete consideration factors and incomplete application of info-gap theory in the existing info-gap theory models.

It is reflected in the following aspects. First, only one uncertainty is usually considered in modeling, such as only load or wind or PV generation uncertainty. Only the uncertainty of wind generation was taken into account in the corresponding problems of References [69, 72, 73, 78, 85, 86, 87]. Only the uncertainty of loads was considered based on info-gap decision theory in [1]. Second, info-gap theory has two performance requirements for uncertainty, namely robustness and opportuneness, but the current research generally ignores opportuneness. For instance, only robustness was taken into account in [1, 79, 83, 86, 87, 77]. Therefore, this paper comprehensively models the uncertainties of wind, PV generation, and loads based on info-gap theory, and develops the optimal multi-objective planning and operation model of the microgrid under risk aversion and risk seeking (opportunity seeking) according to the decision-maker's risk preference, so as to ensure that the decision result is still acceptable when the uncertainty fluctuates arbitrarily within a certain range.

1.3. Contributions

The main contributions of this paper are summarized as follows.

1) In view of the shortcomings of vanilla generative adversarial networks (GANs) and Wasserstein generative adversarial networks (WGANs), such as difficult training, slow convergence rate, and poor sample quality, this paper applies WGAN-GP to wind, PV, and load scenario generation, and utilizes the K-medoids reduction technology to obtain several typical scenarios and reduce the calculation burden. The effect of WGAP-GP is better than that of WGANs, the training of WGAP-GP is stable, and almost no parameters are needed to tune.

2) Because the frequent charging and discharging during the actual use of the BESS results in the actual lifetime of the BESS being lower than the nominal lifetime, this paper considers the actual lifetime of the BESS based on the rain-flow counting algorithm, so as to consider the replacement cost of the BESS. Furthermore, our models take into account dynamic constraints such as power flow and system reliability constraints. The dynamic constraints make our models multi-bus models, which can not only give the total capacity of DERs, but also give the placement of DERs. However, the single-bus aggregate model approach can only give the total number of each component, but it cannot give specific installation locations intrinsically.

3) Based on info-gap theory, the uncertainties of wind, PV generation, and loads are comprehensively considered in optimal microgrid planning and operation. According to decision makers' preference for risk, both a robust planning strategy for risk aversion (RA) and an opportunistic planning strategy for opportunity seeking (OS), or risk seeking, are established, and two different multi-objective bi-level models for the optimal planning and operation of the microgrid planning based on info-gap theory are proposed. Finally, the multi-objective bi-level optimization models are transformed into the single level multi-objective optimization models. These models can provide decision makers with planning schemes for uncertainties of different ranges under different risk attitudes.

4) The correctness, feasibility, superiority, and effectiveness of the proposed models are verified by a bountiful series of numerical examples and analyses, as well as the Monte Carlo method.

The rest of the paper is arranged as follows. Scenario generation and reduction for renewables and loads are elaborated meticulously in Section 2. The BESS lifetime estimation model is described in Section 3. The deterministic microgrid planning and operation model is derived and expounded minutely in Section 4. Multi-objective models for optimal microgrid planning

and operation based on info-gap theory are derived and proposed in great detail in Section 5. Section 6 demonstrates and illustrates the simulation setup and results, and culminates in verification by the Monte Carlo method. Conclusions follow in Section 7.

2. Scenario generation and reduction for renewables and loads

2.1. Scenario generation based on WGAN-GP

WGANs [88] are used to generate renewable scenarios [89]. However, WGANs are sometimes difficult to train, has a slow convergence rate, sometimes does not converge, and sometimes generate poor samples. This is because WGANs use weight clipping to enforce a Lipschitz constraint on the critic. Therefore, this paper adopts WGAN-GP [90] to generate renewable scenarios. WGAN-GP penalizes the norm of gradient of the critic with respect to its input instead of clipping weights. WGAN-GP works better than WGANs, and enables stable training. There is little need to tune hyperparameters for WGAN-GP.

The fundamental framework of WGAN-GP for renewable and load scenario generation is shown in Figure 1. Figure 1 is mainly composed of two deep neural network models, generator G and discriminator D. G and D can be comprised of convolutional neural networks or fully connected neural networks. By learning the potential distribution of historical renewable generation (mainly wind and PV) or load data, the generator G processes the noise signal $\mathbf{z}$ that follows the probability distribution $p_{\mathbf{z}}(\mathbf{z})$ (such as Gaussian distributions) to obtain the generated data $G(\mathbf{z})$ that follows the probability distribution $p_G(\mathbf{z})$. The goal of G is to approximate the probability distribution $G(\mathbf{z})$ of the generated data to the probability distribution $p_{\text{data}}(\mathbf{x})$ of the historical data. The discriminator judges the generated data $G(\mathbf{z})$ of the generator and the historical data $\mathbf{x}$ that follows the probability distribution $p_{\text{data}}(\mathbf{x})$ and outputs the probability $D(G(\mathbf{z}))$ that the generated data $G(\mathbf{z})$ follows the true distribution $p_{\text{data}}(\mathbf{x})$. The goal of D is to determine as accurately as possible whether the input data is historical or generated.

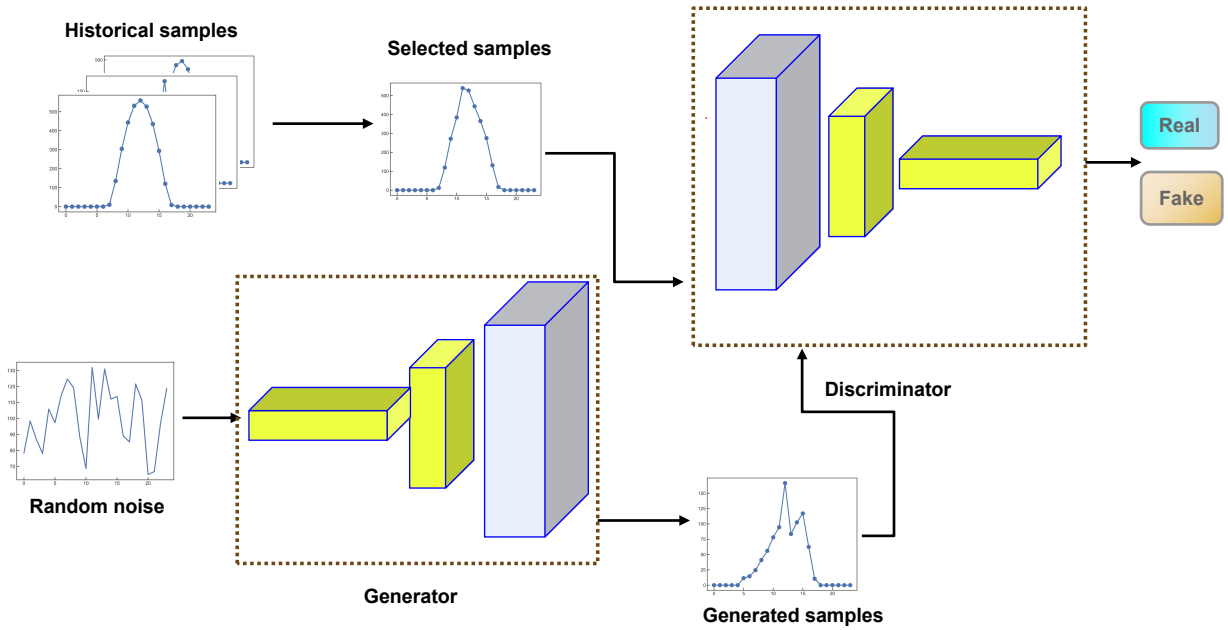

Figure 1: Fundamental framework of WGAN-GP for renewable and load scenario generation.

After defining the training objectives of G and D, it is necessary to construct the loss functions L^G and L^D of G and D respectively for training. For G, a smaller L^G means a higher

probability that the generated data will obey $p_{\text{data}}(\mathbf{x})$. For D, a smaller L^D means that D is better able to distinguish between data sources. L^G and L^D can be represented as follows:

$$L^G = -\mathbb{E}_{\mathbf{z}\sim p_{\mathbf{z}}(\mathbf{z})}[D(G(\mathbf{z}))], \tag{1}$$

$$L^D = \underbrace{-\mathbb{E}_{\mathbf{x}\sim p_{\text{data}}(\mathbf{x})}[D(\mathbf{x})] + \mathbb{E}_{\mathbf{z}\sim p_{\mathbf{z}}(\mathbf{z})}[D(G(\mathbf{z}))]}_{\text{Original discriminator loss}} + \underbrace{\lambda\mathbb{E}_{\hat{\mathbf{x}}\sim p_{\hat{\mathbf{x}}}(\hat{\mathbf{x}})}\left[\left(\|\nabla_{\hat{\mathbf{x}}}D\left(\hat{\mathbf{x}}\right)\|_2 - 1\right)^2\right]}_{\text{Gradient penalty}}, \tag{2}$$

where $\hat{\mathbf{x}} = \xi\mathbf{x} + (1-\xi)G(\mathbf{z}), \xi \sim U[0,1]$, λ represents the weight coefficient of the gradient penalty term, and $\|\cdot\|$ denotes the ℓ_2-norm.

In order to enable simultaneous game training between G and D, we combine (1) and (2) to construct the following minimum-maximization game model about the value function $V(G,D)$:

$$\min_G \max_D V(D,G) = \mathbb{E}_{\mathbf{x}\sim p_{\text{data}}(\mathbf{x})}[D(\mathbf{x})] - \mathbb{E}_{\mathbf{z}\sim p_{\mathbf{z}}(\mathbf{z})}[D(G(\mathbf{z}))] - \lambda\mathbb{E}_{\hat{\mathbf{x}}\sim p_{\hat{\mathbf{x}}}(\hat{\mathbf{x}})}\left[\left(\|\nabla_{\hat{\mathbf{x}}}D\left(\hat{\mathbf{x}}\right)\|_2 - 1\right)^2\right]. \tag{3}$$

In the initial stage of WGAN-GP training, there is a big difference between the data sample generated by G and the real data sample, so D can distinguish the two samples with a high accuracy. In this case, L^D is smaller; however, L^G and $V(G,D)$ are both larger. With the progress of iterations, G adjusts the weight of the generator network to make the generated sample more and more similar to the real sample, and the discriminator network also improves the discriminant ability through learning. This is done through repeated iterations until eventually the discriminator network cannot accurately distinguish the source of the input data sample, at which point the generator is trained and can be used to generate wind, PV, or load scenarios. The detailed procedure of generating renewable scenarios using WGAN-GP is shown in Algorithm 1.

Algorithm 1 WGAN-GP for renewable and load scenario generation

Input: Gradient penalty coefficient λ, number of discriminator iterations per generator iteration $n_{\text{discriminator}}$, batch size m, Adam hyperparameters α, β_1, β_2.
Input: Initial parameters θ_0^D for D and θ_0^G for G.
while θ^G has not converged **do**
  for $t = 1, \cdots, n_{\text{discriminator}}$ **do**
    for $i = 1, \cdots, m$ **do**
      Sample historical data $\mathbf{x} \sim p_{\text{data}}(\mathbf{x})$.
      Sample noise data $\mathbf{z} \sim p_{\mathbf{z}}(\mathbf{z})$ (Gaussian distribution).
      Sample a random number $\xi \sim U[0,1]$.
      $\tilde{\mathbf{x}} \leftarrow G_{\theta^G}(\mathbf{z})$
      $\hat{\mathbf{x}} \leftarrow \xi\mathbf{x} + (1-\xi)\tilde{\mathbf{x}}$
      $L_i^D \leftarrow D_{\theta^D}(\tilde{\mathbf{x}}) - D_{\theta^D}(\mathbf{x}) + \lambda\left(\|\nabla_{\hat{\mathbf{x}}}D_{\theta^D}\left(\hat{\mathbf{x}}\right)\|_2 - 1\right)^2$
    end for
    $\theta^D \leftarrow \text{Adam}\left(\nabla_{\theta^D}\frac{1}{m}\sum_{i=1}^m L_i^D, \theta^D, \alpha, \beta_1, \beta_2\right)$ # Update parameters for D.
  end for
  Sample a batch of noise from Gaussian distribution $\{\mathbf{z}_i\}_{i=1}^m \sim p_{\mathbf{z}}(\mathbf{z})$.
  $\theta^G \leftarrow \text{Adam}\left(\nabla_{\theta^G}\frac{1}{m}\sum_{i=1}^m[-D_{\theta^D}(G_{\theta^G}(\mathbf{z}))], \theta^G, \alpha, \beta_1, \beta_2\right)$ # Update parameters for G.
end while

2.2. Renewable and load scenario reduction based on K-medoids

In order to simplify the problem and improve the computational efficiency, we need to reduce the scenarios generated by WGAN-GP. Assuming that all scenarios before reduction constitute

a set S, the purpose of scenario reduction is to find an optimal subset S' of S to replace S so that S' covers the information contained in S as much as possible, namely:

$$\min \sum_{\substack{\mathbf{p}_i \in S \\ \mathbf{p}_i \notin J}} P_i \min_{\mathbf{p}_j \in J} d_{\mathrm{T}} \left(\mathbf{p}_i, \mathbf{p}_j\right), \tag{4}$$

$$d_{\mathrm{T}}(\mathbf{p}, \mathbf{q}) = \|\mathbf{p} - \mathbf{q}\|_{\mathrm{T}} = \sum_{i=1}^{n} |p_i - q_i|, \tag{5}$$

where P_i is the probability of scenario $\mathbf{p}_i$ appearing, d_{T} is the Manhattan distance between the two scenarios.

Since the traditional scenario reduction methods such as fast forward selection and simultaneous backward reduction [91, 92] are sensitive to the original scenario size, and the clustering algorithm is not as sensitive to the original scenario size as the traditional scenario reduction methods, this paper adopts the K-modiods algorithm to complete the scenario reduction. WGAN-GP may produce some abnormal scenarios when generating scenarios, and the K-means algorithm takes the mean value of sample points in the same class as the clustering center, which is very sensitive to abnormal data. Improper selection of the initial center will lead to poor clustering results, while the K-medoids algorithm takes sample points as clustering centers. The defect of the K-means algorithm is overcome effectively by the K-medoids algorithm, and it has good robustness to outliers. The specific steps of the scene reduction method based on K-medoids are shown in Algorithm 2. Algorithm 2 divides all scenarios into k clusters, and each cluster selects a scenario (medoid) as its representative. The medoid has similar attributes and characteristics with other scenarios in the cluster. Therefore, the attributes and characteristics of renewable and load scenarios after reduction have obvious differences.

Algorithm 2 K-medoids for renewable and load scenario reduction

1: Randomly select k scenarios from S $\{k_0, k_1, \cdots, k_n\}$ as the initial clustering centers.
2: **while** The medoids have not converged or the maximum number of iterations have not been reached **do**
3: The remaining scenarios are assigned to the clusters represented by the current best medoids based on the principle of the closest Manhattan distance (5) to the medoids.
4: In each cluster, calculate the criterion problem (4) corresponding to each member point, and select the point corresponding to the minimum criterion function as the new medoids.
5: **end while**

3. BESS lifetime estimation model

In the economic analysis of the microgrid design, the lifetime of the BESS is an important factor for its investment cost analysis. However, the lifetime prediction of the BESS is a core and intractable problem in the research of the BESS. The lifetime of the BESS is closely related to its working environment, charging and discharging cut-off voltages, currents, depths of discharge (DoD)[1], charging and discharging cycles, and other factors. The lifetime of the Li-ion battery is mainly affected by the ambient temperature and the DoD. At the same ambient temperature, the greater the DoD of the BESS, the shorter the lifetime. Generally, the operating temperature and charging current are related to the heat dissipation and control system. Since the ambient temperature is regarded as the room temperature and the battery is assumed to operate within

[1]The DoD of the BESS refers to the percentage of discharging energy released by the BESS to its rated capacity during a complete charge-discharge cycle.

a certain range of conditions, we only considers the influence of the DoD of the BESS on its lifetime.

It should be noted that a complete (full) cycle is composed of a discharge half cycle and a charge half cycle. As shown in Figure 2, the circles of $\mathrm{SoC}_1(\tau_0) \to \mathrm{SoC}_1(\tau_1) \to \mathrm{SoC}_1(\tau_2)$ and $\mathrm{SoC}_2(\tau_0) \to \mathrm{SoC}_2(\tau_1) \to \mathrm{SoC}_2(\tau_2)$ are full circles, and the circles of $\mathrm{SoC}_1(\tau_0) \to \mathrm{SoC}_1(\tau_1)$ and $\mathrm{SoC}_1(\tau_1) \to \mathrm{SoC}_1(\tau_2)$ are half cycles. The DoD of $\mathrm{SoC}_1(\tau_0) \to \mathrm{SoC}_1(\tau_1) \to \mathrm{SoC}_1(\tau_2)$ is $|\mathrm{SoC}_1(\tau_0) - \mathrm{SoC}_1(\tau_1)|$.

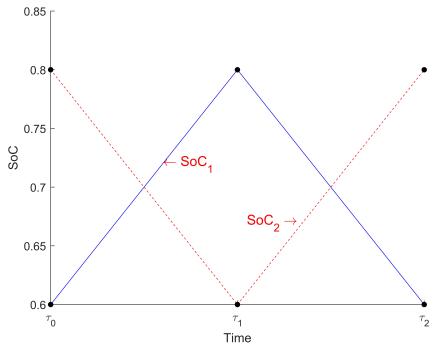

Figure 2: Demonstration of full circles.

3.1. Calculating the DoD using the rainflow counting algorithm

Due to the irregular variations of the state of charge (SoC) in practical engineering, a clear charging and discharging cycle cannot be directly divided. Therefore, the first problem we need to solve is how to divide the SOC curve and get the charging-discharging cycle sequences with clear physical significance. In this paper, the rainflow counting algorithm [93, 94] is used to determine a series of cycles in the SOC curve and the DoD of each cycle, and then calculate the equivalent cycle lifetime of the battery according to the corresponding relationship between the DoD and the lifetime. The specific rules and main steps of the rain-flow counting algorithm are shown in Algorithm 3.

Algorithm 3 Rain-flow counting algorithm

1: Turn the SOC curve clockwise by 90° and mark the starting point, local maximums, and local minimums in the SOC curve.
2: Rain drops flow downward from the starting point, local maximums, and local minimums. At the same time, rain drops fall vertically when they reach local maximums and local minimums. When a rain drop meets a new local maximum larger than the original local maximum or a new local minimum smaller than the original local minimum, it stops falling.
3: When a rain drop meets the rain drop falling from the high roof, it stops flowing and forms a full cycle.
4: Determine each full cycle and half cycle.
5: The amplitude of each cycle is taken as the DoD of the cycle.

Assume that the SOC curve of a BESS over a period of time is shown in Figure 3. After counting the extreme value points of the SOC curve and conducting numbering these points, the SOC curve extremum point plot can be obtained as shown in Figure 4. Based on the rain-flow counting algorithm, the schematic diagram of each cycle and the DoD of each cycle are shown in Figure 4 and Table 1, respectively.

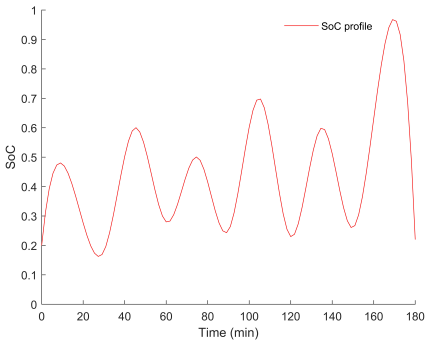

Figure 3: SoC curve of a BESS.

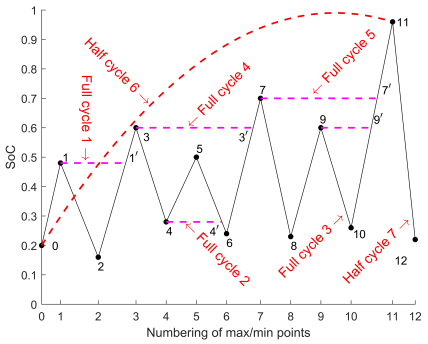

Figure 4: Extremum points and each cycle of the SoC curve.

Table 1: DoD of each cycle

Cycle No.	Full Cycle 1	Full Cycle 2	Full Cycle 3	Full Cycle 4	Full Cycle 5	Half Cycle 6	Half Cycle 7
DoD	0.32	0.22	0.34	0.36	0.47	0.76	0.74

Table 2: Relationship between the DoD and the number of cycles to failure

DoD (%)	Number of cycles to failure
10	70000
20	31000
30	18100
40	11800
50	8100
60	5800
70	4300
80	3300
90	2500

3.2. Equivalent BESS lifetime estimation

The relationship between the DoD and the number of cycles to failure of a BESS is shown in Table 2 [95].

The polynomial function is used to fit the data in Table 2, and the relationship between the DoD and the number of cycles to failure is

$$\begin{aligned} N_{\text{cf}} =& 5.12 \times 10^6 \text{DoD}^6 - 1.7749 \times 10^7 \text{DoD}^5 + 2.4964 \times 10^7 \text{DoD}^4 - 1.8303 \times 10^7 \text{DoD}^3 \\ &+ 7.471 \times 10^6 \text{DoD}^2 - 1.672 \times 10^6 \text{DoD} + 1.78 \times 10^5, \end{aligned} \tag{6}$$

where N_{cf} is the number of cycles to failure. The corresponding fitted curve is shown in Fig. 5.

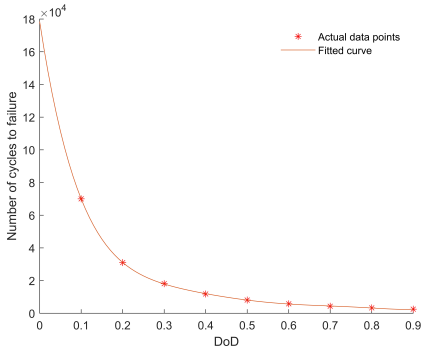

Figure 5: Relationship curve between the DoD and the number of cycles.

Assume that the number of cycles of the SoC of a BESS in a day is n, and the DoDs corresponding to all cycles are $\text{DOD}_1, \text{DOD}_2, \cdots, \text{DOD}_n$, respectively. The number of cycles to failure corresponding to DOD_i is $N_{i,\text{cf}}$, then $1/N_{i,\text{cf}}$ represents the lifetime loss rate in the ith cycle. The lifetime loss of the BESS in one day is

$$L_{\text{BESS}} = \sum_{i=1}^{n} \frac{1}{N_{i,\text{cf}}}. \tag{7}$$

Then, the BESS lifetime in years can be calculated using the following formula:

$$T_{\text{BESS}} = \frac{1}{365 L_{\text{BESS}}}. \tag{8}$$

4. Problem formulation

The considered DERs in the paper include WTs, PV panels, diesel generators (DGs), BESSs, i.e., $\Omega_{\text{RES}} = \{\text{WTs}, \text{PVs}\}$, $\Omega_{\text{DFG}} = \{\text{DEs}\}$, $\Omega_{\text{ESS}} = \{\text{BESSs}\}$, and $\Omega_{\text{DER}} = \Omega_{\text{RES}} \cup \Omega_{\text{DFG}} \cup \Omega_{\text{ESS}}$. The BESSs used in this paper are Li-ion BESSs. By minimizing the annualized equivalent investment and operation costs, the deterministic microgrid planning and operation model is constructed in this section.

4.1. Objective function

The optimization objective is to minimize the total annualized investment and operation cost of the microgrid, which consists of the cost of the initial investment of equipment, the cost of BESS and other equipment replacement, the operation and maintenance (OM) cost, the emission cost, the cost of the electricity purchased from the main grid, the electricity export revenue, and the load curtailment cost. The chosen time-step Δt is one hour, so energy and power are numerically identical. The fundamental objective can be formulated as follows:

$$\min C = C_{\text{inv}} + C_{\text{op}}, \tag{9}$$

$$C_{\text{inv}} = C_{\text{acq}} + C_{\text{OM}} + C_{\text{ins}} + C_{\text{rep}}, \tag{10}$$

$$C_{\text{op}} = C_{\text{gen}} + C_{\text{emi}} + C_{\text{imp}} - C_{\text{exp}} + C_{\text{cur}}, \tag{11}$$

$$C_{\text{acq}} = \sum_{n\in\mathcal{N}} \sum_{l\in\Omega_{\text{DER}}} a^l X_n^l \frac{r\left(1+r\right)^T}{\left(1+r\right)^T - 1}, \tag{12}$$

$$r = \frac{i-f}{1+f}, \tag{13}$$

$$C_{\text{ins}} = \sum_{n\in\mathcal{N}} \sum_{l\in\Omega_{\text{DER}}} B_n^l \text{FC}^l \frac{r\left(1+r\right)^T}{\left(1+r\right)^T - 1}, \tag{14}$$

$$C_{\text{rep}} = \sum_{n\in\mathcal{N}} \sum_{l\in\Omega_{\text{DER}}} a^l X_n^l \left(\frac{T}{T^l} - 1\right) \frac{r\left(1+r\right)^T}{\left(1+r\right)^T - 1}, \tag{15}$$

$$C_{\text{OM}} = \sum_{n\in\mathcal{N}} \sum_{l\in\Omega_{\text{DER}}} \text{OM}^l P_{\text{max}}^l X_n^l, \tag{16}$$

$$C_{\text{gen}} = \frac{365}{D} \sum_{d=1}^{D} \sum_{h=1}^{H} \sum_{n\in\mathcal{N}} \sum_{l\in\Omega_{\text{DFG}}} g^l P_{n,d,h}^l, \tag{17}$$

$$C_{\text{emi}} = \frac{365}{D} \sum_{d=1}^{D} \sum_{h=1}^{H} \sum_{n\in\mathcal{N}} \sum_{l\in\Omega_{\text{DFG}}} \sum_{e=1}^{m} \pi^e \mu^{l,e} P_{n,d,h}^l, \tag{18}$$

$$C_{\text{imp}} = \frac{365}{D} \sum_{d=1}^{D} \sum_{h=1}^{H} r_h^{\text{imp}} P_{\text{PCC},d,h}^{\text{imp}}, \tag{19}$$

$$C_{\text{exp}} = \frac{365}{D} \sum_{d=1}^{D} \sum_{h=1}^{H} r_h^{\text{exp}} P_{\text{PCC},d,h}^{\text{exp}}, \tag{20}$$

$$C_{\text{cur}} = \frac{365}{D} \rho \sum_{d=1}^{D} \sum_{h=1}^{H} \sum_{n\in\mathcal{N}} P_{n,d,h}^{\text{lc}}. \tag{21}$$

where C, C_{inv}, C_{op}, C_{acq}, C_{OM}, C_{ins}, C_{rep}, C_{gen}, C_{emi}, C_{imp}, C_{exp}, and C_{cur} are the total annualized investment and operation costs, the annualized investment cost, the annualized operation cost, the annualized DER acquisition cost, the annualized DER OM cost, the annualized DER installation cost, the annualized DER replacement cost, the annualized DER generation cost, the annualized DER emission cost, the annualized cost of electricity imported from the main grid, the annualized revenue of the electricity exported to the main grid, and the annualized cost of load curtailment, respectively. B_n^l is the binary decision variable for DER l at bus n. FC^l is the fixed installation cost of DER l. d, e, h, l, n, and t stand for indices of days, pollutants, hours, DERs, buses, and optimization periods or time, respectively. $\mathcal{N}$ is the set of buses. $\mu^{l,e}$ is the pollutant e emission coefficient of DFG l. π^e and ρ are unit penalty costs of pollutant e and load curtailment, respectively. a^l is the acquisition cost of DER l. OM^l is the OM cost of DFG l. r, i, and f are the real discount rate, the nominal discount rate, and the expected inflation rate, respectively. D is the number of typical days in a year. H is the total hours in a day. g^l is the unit generation cost of DFG l. m is the total types of pollutants. T is the project lifetime. T^l is the actual lifetime of DER l (BESSs or other DERs). r_t^{exp} and r_t^{imp} are electricity rates for electricity export and import during period t, respectively. X_j^l is the number of DER l installed at bus j. P_{max}^l is the capacity of DER l.

4.2. Constraints

4.2.1. Power flow constraints

Linearized distribution flow (LinDistFlow) [96] is adopted in this paper to integrate power flow into the network.

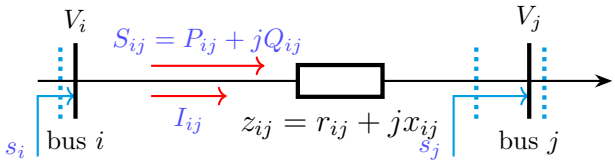

Figure 6: A radial network with 2-bus

Considering the network shown in Figure 6, we have the following equations:

$$\sum_{k:j\to k} P_{jk,t} = \sum_{l\in\Omega_{\mathrm{DER}}} P^{l}_{j,t} + P^{\mathrm{lc}}_{j,t} - P^{\mathrm{ld}}_{j,t} + \sum_{i:i\to j} \left(P_{ij,t} - 3r_{ij}\ell_{ij,t}\right), \quad \forall j \in \mathcal{N}, \forall t \in \mathcal{T}, \tag{22}$$

$$\begin{aligned}\sum_{k:j\to k} Q_{jk,t} = &\left(\sum_{l\in\Omega_{\mathrm{DER}}} P^{l}_{j,t} + P^{\mathrm{lc}}_{j,t} - P^{\mathrm{ld}}_{j,t}\right)\tan(\arccos(pf)) \\ &+ \sum_{i:i\to j} \left(Q_{ij,t} - 3x_{ij}\ell_{ij,t}\right), \quad \forall j \in \mathcal{N}, \forall t \in \mathcal{T},\end{aligned} \tag{23}$$

$$\nu_{j,t} = \nu_{i,t} - 2\left(r_{ij}P_{ij,t} + x_{ij}Q_{ij,t}\right) + 3\left(r^2_{ij} + x^2_{ij}\right)\ell_{ij,t}, \quad \forall ij \in \mathcal{E}, \forall t \in \mathcal{T}, \tag{24}$$

$$3\ell_{ij,t} = \frac{P^2_{ij,t} + Q^2_{ij,t}}{\nu_{i,t}}, \quad \forall ij \in \mathcal{E}, \forall \in t, \tag{25}$$

where $\mathcal{E}$ is the set of branches. r_{ij}, x_{ij}, and z_{ij} are the resistance, the reactance, and the impedance on line ij, respectively. pf is the power factor. $P^{l}_{j,t}$ is the injected active power generated by DER l at bus j at time t. $P_{ij,t}$ and $Q_{ij,t}$ are the active and reactive power from buses i to j at time t (sending–ending), respectively. $P^{\mathrm{lc}}_{j,t}$ and $Q^{\mathrm{lc}}_{j,t}$ are the curtailed active and reactive loads at bus j at time t, respectively. $P^{\mathrm{ld}}_{j,t}$ and $Q^{\mathrm{ld}}_{j,t}$ are the active and reactive power of the load at bus j at time t, respectively. $\nu_{j,t}$ is the square of the magnitude of the complex voltage at bus j during period t, i.e., $\nu_{j,t} := |V_{j,t}|^2$. $\ell_{ij,t}$ is the square of the magnitude of the complex current from buses i to j during period t, i.e., $\ell_{ij,t} := |I_{ij,t}|^2$.

Remark 1. *Equations (22)–(25) use the actual value, and the power in the equations is the three-phase power. If the actual value of the single-phase power or the per value is adopted, the coefficient* 3 *should be removed from the above four formulae.*

If we remove $3r_{ij}\ell_{ij,t}$, $3x_{ij}\ell_{ij,t}$, and $3\left(r^2_{ij} + x^2_{ij}\right)\ell_{ij,t}$ from (22), (23), and (24), respectively, we can obtain the linearized *branch flow model* or *LinDistFlow*, which can greatly improve the solving speed:

$$\sum_{k:j\to k} P_{jk,t} = \sum_{l\in\Omega_{\mathrm{DER}}} P^{l}_{j,t} + P^{\mathrm{lc}}_{j,t} - P^{\mathrm{ld}}_{j,t} + \sum_{i:i\to j} P_{ij,t}, \quad \forall j \in \mathcal{N}, \forall t \in \mathcal{T}, \tag{26}$$

$$\begin{aligned}\sum_{k:j\to k} Q_{jk,t} = &\left(\sum_{l\in\Omega_{\mathrm{DER}}} P^{l}_{j,t} + P^{\mathrm{lc}}_{j,t} - P^{\mathrm{ld}}_{j,t}\right)\tan(\arccos(pf)) \\ &+ \sum_{i:i\to j} Q_{ij,t}, \quad \forall j \in \mathcal{N}, \forall t \in \mathcal{T},\end{aligned} \tag{27}$$

$$\nu_{j,t} = \nu_{i,t} - 2\left(r_{ij}P_{ij,t} + x_{ij}Q_{ij,t}\right), \quad \forall ij \in \mathcal{E}, \forall t \in \mathcal{T}. \tag{28}$$

In order to ensure the safe and stable operation of the system, the following variable bounds must also be met:

$$F_l^{\min} \leq P_{ij,t} \leq F_l^{\max}, \quad \forall i \in \mathcal{N}, \forall j \in \mathcal{N}, \forall t \in \mathcal{T}, i \neq j, \tag{29}$$

$$|\underline{V}|^2 \leq \nu_{j,t}, \leq \left|\overline{V}\right|^2, \quad \forall j \in \mathcal{N}, \forall t \in \mathcal{T}, \tag{30}$$

$$0 \leq \ell_{ij,t} \leq \left|\overline{I}_{ij}\right|^2, \quad \forall j \in \mathcal{N}, \forall t \in \mathcal{T}, \tag{31}$$

where $F_l^{\min}$ and $F_l^{\max}$ are the minimum and maximum power flow limits for line l, respectively. $|\underline{V}|$ and $|\overline{V}|$ are the minimum and maximum acceptable voltage magnitude thresholds, respectively. $|\overline{I}_{ij}|$ is the maximum acceptable magnitude of the complex current from buses i to j.

4.2.2. BESS constraints

According to the principle of energy conservation, the charging and discharging of the BESS at any time period t satisfy (32) and (33), respectively:

$$E_{j,t}^{\text{BESS}} = (1-\delta)E_{j,t-1}^{\text{BESS}}\Delta t + \eta^{\text{BESS}+}P_{j,t}^{\text{BESS}+}\Delta t, \quad \forall j \in \mathcal{N}, \forall t \in \mathcal{T}, \tag{32}$$

$$E_{j,t}^{\text{BESS}} = (1-\delta)E_{t-1}^{\text{BESS}}\Delta t - \frac{P_{j,t}^{\text{BESS}-}\Delta t}{\eta^{\text{BESS}-}}, \quad \forall j \in \mathcal{N}, \forall t \in \mathcal{T}, \tag{33}$$

where $E_{j,t}^{\text{BESS}}$ is the remaining available capacity (stored energy) of the BESS at bus j at the end of period t. δ is the self-discharging rate of the BESS. $\eta^{\text{BESS}-}$ and $\eta^{\text{BESS}+}$ are the discharging and charging efficiency of the BESS, respectively. $P_{j,t}^{\text{BESS}+}$ is the power charged by the grid to the BESS at bus j during period t. $P_{j,t}^{\text{BESS}-}$ is the power discharged by the BESS during at bus j during period t.

The BESS cannot be charged and discharged at the same time:

$$P_{j,t}^{\text{BESS}+}P_{j,t}^{\text{BESS}-} = 0, \quad \forall j \in \mathcal{N}, \forall t \in \mathcal{T}. \tag{34}$$

To prevent the BESS from overheating on account of excessive charging and discharging power, which may affect its service life, the following requirements must be met:

$$0 \leq P_{j,t}^{\text{BESS}+} \leq \frac{X_j^{\text{BESS}}P_{\max}^{\text{BESS}}}{\eta^{\text{BESS}+}}, \quad \forall j \in \mathcal{N}, \forall t \in \mathcal{T}, \tag{35}$$

$$0 \leq P_{j,t}^{\text{BESS}-} \leq \eta^{\text{BESS}-}X_j^{\text{BESS}}P_{\max}^{\text{BESS}}, \quad \forall j \in \mathcal{N}, \forall t \in \mathcal{T}. \tag{36}$$

The state of charge (SoC)[2] of the BESS must satisfy

$$SoC_{j,\min} \leq SoC_{j,t} \leq SoC_{j,\max}, \quad \forall j \in \mathcal{N}, \forall t \in \mathcal{T} \tag{37}$$

$$SoC_{j,t} = \frac{E_{j,t}^{\text{BESS}}}{X_j^{\text{bat}}E_{\max}^{\text{bat}}}, \quad \forall j \in \mathcal{N}, \forall t \in \mathcal{T}, \tag{38}$$

where $SoC_{j,\min}$ and $SoC_{j,\max}$ minimum and maximum acceptable SoC at bus j, respectively. $SoC_{j,t}$ is the SoC at bus j at the end of period t, and $E_{\max}^{\text{BESS}}$ is the BESS storage capacity.

Generally, the SoC of the BESS at the end of each dispatching period is consistent with the beginning of the dispatching period, that is, the following formula must be satisfied:

$$SoC_{j,0} = SoC_{j,H}. \tag{39}$$

[2]The SoC of the BESS is the ratio of its remaining charge to its capacity.

Constraint (34) is bilinear and Constraint (38) has the form of x/y. They are all strongly non-convex and non-linear. We must relax them in order to make the computation tractable. Constraint (34) is converted into the following mixed integer linear constraints:

$$0 \leq P_{j,t}^{\mathrm{BESS-}} \leq B_{j,t}^{\mathrm{BESS-}} \eta^{\mathrm{BESS-}} X_{j,\max}^{\mathrm{bat}} P_{\max}^{\mathrm{bat}}, \quad \forall j \in \mathcal{N}, \forall t \in \mathcal{T}, \tag{40}$$

$$0 \leq P_{j,t}^{\mathrm{BESS+}} \leq \frac{\left(1 - B_{j,t}^{\mathrm{BESS-}}\right) X_{j,\max}^{\mathrm{bat}} P_{\max}^{\mathrm{bat}}}{\eta^{\mathrm{BESS+}}}, \quad \forall j \in \mathcal{N}, \forall t \in \mathcal{T}. \tag{41}$$

Furthermore, (32)–(33) are *if-esle* constraints. However, the existing solver cannot tackle such constraints, which can be eliminated by using the Big-M method. Constraints (32)–(33) can be modified into the following mixed integer linear constraints:

$$\begin{aligned} &(1-\delta) E_{j,t-1}^{\mathrm{BESS}} + \eta^{\mathrm{BESS+}} P_{j,t}^{\mathrm{BESS+}} \Delta t - B_{j,t}^{\mathrm{BESS-}} M \leq E_{j,t}^{\mathrm{BESS}} \\ &\leq (1-\delta) E_{j,t-1}^{\mathrm{BESS}} + \eta^{\mathrm{BESS+}} P_{j,t}^{\mathrm{BESS+}} \Delta t + B_{j,t}^{\mathrm{BESS-}} M, \quad \forall j \in \mathcal{N}, \forall t \in \mathcal{T}, \end{aligned} \tag{42}$$

$$\begin{aligned} &(1-\delta) E_{j,t-1}^{\mathrm{BESS}} - \frac{P_{j,t}^{\mathrm{BESS-}} \Delta t}{\eta^{\mathrm{BESS-}}} - \left(1 - B_{j,t}^{\mathrm{BESS-}}\right) M \leq E_{j,t}^{\mathrm{BESS}} \\ &\leq (1-\delta) E_{j,t-1}^{\mathrm{BESS}} - \frac{P_{j,t}^{\mathrm{BESS-}} \Delta t}{\eta^{\mathrm{BESS-}}} + \left(1 - B_{j,t}^{\mathrm{BESS-}}\right) M, \quad \forall j \in \mathcal{N}, \forall t \in \mathcal{T}. \end{aligned} \tag{43}$$

Remark 2. *M is some sufficiently large positive number, i.e. $M \gg 0$, but not an infinite positive number. Pay attention to the value of M: neither too small nor too large. Taking too small may lead to an infeasible solution. It should not be very large in order to avoid convergence problems. Thus, it is best to make it as small as possible if constraints satisfied. In our case, we can choose it on the basis of the upper bound of the installation number of the BESS.*

In order to eliminate the non-convex x/y of (38), (37) and (38) can be converted into the equations as follows:

$$\mathrm{SoC}_{j,\min} X_j^{\mathrm{bat}} E_{\max}^{\mathrm{bat}} \leq E_{j,t}^{\mathrm{BESS}} \leq \mathrm{SoC}_{j,\max} X_j^{\mathrm{bat}} E_{\max}^{\mathrm{bat}}, \quad \forall j \in \mathcal{N}, \forall t \in \mathcal{T}. \tag{44}$$

4.2.3. Generation and load shedding constraints

The following formulae should be met for different generation technologies:

$$0 \leq P_{j,t}^{l} \leq X_j^{l} A_t^{l}, \quad \forall j \in \mathcal{N}, \forall t \in \mathcal{T}, \forall l \in \Omega_{\mathrm{RES}}, \tag{45}$$

$$X_j^{l} P_{\min}^{l} \leq P_{j,t}^{l} \leq X_j^{l} P_{\max}^{l}, \forall j \in \mathcal{N}, \forall t \in \mathcal{T}, \forall l \in \Omega_{\mathrm{DFG}}, \tag{46}$$

$$-RD^{l} \leq P_{j,t}^{l} - P_{j,t-1}^{l} \leq RU^{l}, \quad \forall j \in \mathcal{N}, \forall (t-1) \in \mathcal{T}, \forall l \in \Omega_{\mathrm{DFG}}, \tag{47}$$

$$0 \leq P_{j,t}^{\mathrm{lc}} \leq P_{j,\max}^{\mathrm{lc}}, \quad \forall j \in \mathcal{N}, \forall t \in \mathcal{T}, \tag{48}$$

$$0 \leq \sum_{j=1}^{|\mathcal{N}|} X_j^{l} \leq X_{\max}^{l}, \quad \forall l \in \Omega_{\mathrm{DER}}, \tag{49}$$

$$P_{j,t}^{l}, P_{j,t}^{\mathrm{lc}} \in \mathbb{R}_{+}, \quad \forall j \in \mathcal{N}, \forall t \in \mathcal{T}, \forall l \in \Omega_{\mathrm{RES}} \cup \Omega_{\mathrm{DFG}}, \tag{50}$$

$$X_j^{l} \in \mathbb{Z}_{+}, \quad j \in \mathcal{N}, l \in \Omega_{\mathrm{DER}}, \tag{51}$$

where $P_{\min}^{l}$ is the minimum allowable output power of DFG l. RD^{l} and RU^{l} are ramp down and ramp up rates of DER l ($l \in \Omega_{\mathrm{DFG}}$), respectively. A_t^{l} are the predicted output of DER l ($l \in \Omega_{\mathrm{RES}}$) during period t. $P_{j,\max}^{\mathrm{lc}}$ is the maximum load allowed to be shed at bus j. $X_{\max}^{l}$ is the upper limit of installation of DER l.

In (45), the output of RESs is limited by their available capacities. Constraint (46) guarantees that the dispatch of each DFG is within the allowable generation range. Hourly ramping capability of each DFG is constrained by (47). Constraint (48) secures that the curtailed load at each bus does not exceed the maximum allowable shed load. The total installation number of each DER at all buses is constrained by (49).

4.2.4. Import and export constraints

Suffice it to say that power cannot be exported to the grid and imported from the grid at the point of common coupling (PCC) simultaneously, that is, the following equation must be satisfied:

$$0 \le P^{\text{imp}}_{\text{PCC},t} \le B_{\text{PCC},t} P_{\text{PCC,max}}, \quad \forall t \in \mathcal{T}, \tag{52}$$

$$0 \le P^{\text{exp}}_{\text{PCC},t} \le (1 - B_{\text{PCC},t})\, P_{\text{PCC,max}}, \quad \forall t \in \mathcal{T}, \tag{53}$$

where $P_{\text{PCC,max}}$ is the maximum exchange power between the microgrid and the main grid. $B_{\text{PCC},t}$ is "1" if the microgrid import the power from the grid during period t and "0" otherwise. $P^{\text{exp}}_{\text{PCC},t}$ is the power exported to the main grid at the PCC during period t, and $P^{\text{imp}}_{\text{PCC},t}$ is power imported from the main grid at the PCC during period t.

4.2.5. Reliability constraints

In order to ensure the critical loads are supplied all the time, the following constraints should be satisfied:

$$\sum_{n \in \mathcal{N}} P^{l}_{n} \ge \sum_{n \in \mathcal{C}} P^{\text{load}}_{n,t}, \forall t, \forall l \in \{\text{WTs}, \text{PVs}, \text{DGs}\}, \tag{54}$$

where $\mathcal{C}$ is the set of critical load buses.

4.3. Deterministic microgrid planning and operation model

From the above discussions, the deterministic microgrid planning and operation model can be summarized as follows:

$$\begin{aligned} \min \quad & C = C_{\text{inv}} + C_{\text{op}} \\ \text{s.t.} \quad & (10)\text{–}(21),\ (26)\text{–}(31),\ (35)\text{–}(36),\ (39)\text{–}(54). \end{aligned} \tag{55}$$

Problem (55) is also known as the risk-neutral model.

5. Multi-objective models for optimal microgrid planning and operation based on info-gap theory

5.1. Modeling uncertainty by info-gap theory

Because the robustness model based on info-gap theory sets the expected cost or profit index, both system robustness and basic economy can be guaranteed, which is better than the traditional robust optimization method. Unlike rigorously exact sets of upper and lower bounds in robust optimization, the uncertainties of info-gap theory are modeled as an imprecise set and described by the uncertainty sets of some non-probabilistic models, such as envelope-bound models, slope-bound models, and energy-bound models. In the light of the characteristics of the uncertainties of wind, PV generation, and loads, the envelope-bound model is adopted in this paper. The uncertainty sets of wind, PV generation, and loads can be expressed as

$$\mathcal{U}(\alpha_{\text{WT}}, \tilde{P}^{\text{WT}}_{j,t}) := \left\{ P^{\text{WT}}_{j,t} \,\middle|\, \left| P^{\text{WT}}_{j,t} - \tilde{P}^{\text{WT}}_{j,t} \right| \le \alpha_{\text{WT}} \tilde{P}^{\text{WT}}_{j,t} \right\}, \tag{56}$$

$$\mathcal{U}(\alpha_{\text{PV}}, \tilde{P}^{\text{PV}}_{j,t}) := \left\{ P^{\text{PV}}_{j,t} \,\middle|\, \left| P^{\text{PV}}_{j,t} - \tilde{P}^{\text{PV}}_{j,t} \right| \le \alpha_{\text{PV}} \tilde{P}^{\text{PV}}_{j,t} \right\}, \tag{57}$$

$$\mathcal{U}(\alpha_{\text{load}}, \tilde{P}^{\text{load}}_{j,t}) := \left\{ P^{\text{load}}_{j,t} \,\middle|\, \left| P^{\text{load}}_{j,t} - \tilde{P}^{\text{load}}_{j,t} \right| \le \alpha_{\text{load}} \tilde{P}^{\text{load}}_{j,t} \right\}, \tag{58}$$

$$\alpha_{\text{WT}} \ge 0,\ \alpha_{\text{PV}} \ge 0,\ \alpha_{\text{load}} \ge 0, \tag{59}$$

where $\tilde{P}^{\text{WT}}_{j,t}$, $\tilde{P}^{\text{PV}}_{j,t}$, and $\tilde{P}^{\text{load}}_{j,t}$ are the forecast values of wind, PV generation, and loads, respectively. $P^{\text{WT}}_{j,t}$, $P^{\text{PV}}_{j,t}$, $P^{\text{load}}_{j,t}$ are the actual values of wind, PV generation, and loads, respectively.

α_{WT}, α_{PV}, and α_{load} are the radii (horizons) of the uncertainties of wind, PV generation, and loads, respectively.

Considering that the risk attitude of decision makers will affect the final benefits and planning schemes of the microgrid, in this paper, a robustness model (RM) with RA and an opportunity model (OM) with OS are established. The former develops a multi-objective model under the RA strategy for decision makers with more conservative decision intention, while the latter a multi-objective model under the OS strategy for decision makers with more speculative decision intention.

5.2. A multi-objective RM with RA

Obviously, the uncertain variables should satisfy the following constraints:

$$P_{j,t}^{\mathrm{WT}} \in \mathcal{U}(\alpha_{\mathrm{WT}}, \tilde{P}_{j,t}^{\mathrm{WT}}), \tag{60}$$

$$P_{j,t}^{\mathrm{PV}} \in \mathcal{U}(\alpha_{\mathrm{PV}}, \tilde{P}_{j,t}^{\mathrm{PV}}), \tag{61}$$

$$P_{j,t}^{\mathrm{load}} \in \mathcal{U}(\alpha_{\mathrm{load}}, \tilde{P}_{j,t}^{\mathrm{load}}). \tag{62}$$

The RM model achieves the robustness while ensuring the basic economy, that is, the RM model maximizes uncertainty on the premise that the decision cost does not exceed the expected value. The greater the value of uncertainty, the greater the RM ability, but the greater the corresponding planning and scheduling cost. The decision makers gain the ability to avoid risks at the cost of more planning and operation costs. The proposed multi-objective RM model is formulated as follows:

$$\begin{aligned} \max \quad & (\alpha_{\mathrm{WT}}, \alpha_{\mathrm{PV}}, \alpha_{\mathrm{load}}) \\ \text{s.t.} \quad & \max C \leq (1+\delta)\, C_0 \\ & \text{s.t.}(9)\text{–}(21),\ (26)\text{–}(31),\ (35)\text{–}(36),\ (39)\text{–}(54),\ (56)\text{–}(62), \end{aligned} \tag{63}$$

where δ is the robust level factor, which is proportional to the risk avoidance degree. $C_0 = \min C|(\boldsymbol{\rho} = \tilde{\boldsymbol{\rho}})$ is the base cost, which represents the minimum value of C when $P_{j,t}^{\mathrm{WT}} = \tilde{P}_{j,t}^{\mathrm{WT}}$, $P_{j,t}^{\mathrm{PV}} = \tilde{P}_{j,t}^{\mathrm{PV}}$, and $P_{j,t}^{\mathrm{load}} = \tilde{P}_{j,t}^{\mathrm{load}}$. That is, C_0 is the optimal value of Problem (55).

The RM model deems that uncertainty will affect the planning result of the microgrid. The greater the uncertainty in the RM model, the less sensitive the corresponding decision scheme is to the uncertainty, that is, the better the robustness.

5.3. A multi-objective OM with OS

The OM holds that uncertainty can benefit planning and scheduling. In the OS strategy, the objective is to minimize uncertainty and the risks brought by uncertainty, so as to obtain greater benefits. The OS strategy ensures that the obtained limit values of uncertainty parameter fluctuations make the total cost of microgrid planning and operation not greater than the expected cost. The established OM model can be expressed as follows:

$$\begin{aligned} \min \quad & (\alpha_{\mathrm{WT}}, \alpha_{\mathrm{PV}}, \alpha_{\mathrm{load}}) \\ \text{s.t.} \quad & \min C \leq (1-\kappa)\, C_0 \\ & \text{s.t.}(9)\text{–}(21),\ (26)\text{–}(31),\ (35)\text{–}(36),\ (39)\text{–}(54),\ (56)\text{–}(62), \end{aligned} \tag{64}$$

where κ is the opportunistic level factor.

In the OM model, the smaller the uncertainty, the more likely the corresponding decision scheme is to produce favorable results.

5.4. Model transformation

5.4.1. RM

Constraints (60)–(62) in RM can be converted to

$$P_{j,t}^{\mathrm{WT}} = (1-\alpha_{\mathrm{WT}})\tilde{P}_{j,t}^{\mathrm{WT}}, \tag{65}$$

$$P_{j,t}^{\mathrm{PV}} = (1-\alpha_{\mathrm{PV}})\tilde{P}_{j,t}^{\mathrm{PV}}, \tag{66}$$

$$P_{j,t}^{\mathrm{load}} = (1+\alpha_{\mathrm{load}})\tilde{P}_{j,t}^{\mathrm{load}}. \tag{67}$$

Problem (63) is a multi-objective bi-level problem, which can be converted to the following multi-objective single level problem:

$$\begin{aligned} \max \quad & (\alpha_{\mathrm{WT}}, \alpha_{\mathrm{PV}}, \alpha_{\mathrm{load}}) \\ \text{s.t.} \quad & C \le (1+\delta)\, C_0 \\ & (9)\text{–}(21),\ (26)\text{–}(31),\ (35)\text{–}(36),\ (39)\text{–}(54),\ (59),\ (65)\text{–}(67). \end{aligned} \tag{68}$$

In order to keep the model within the framework of classical mathematics, this paper adopts the ϵ-constraint method instead of evolutionary algorithms to solve the above multi-objective problem. Finally, Problem (63) can be transformed into the following problem:

$$\begin{aligned} \max \quad & \alpha_{\mathrm{PV}} \\ \text{s.t.} \quad & \alpha_{\mathrm{WT}} \ge \epsilon_{\mathrm{WT},i} \\ & \alpha_{\mathrm{load}} \ge \epsilon_{\mathrm{load},i}, \\ & \epsilon_{\mathrm{WT},i} = \epsilon_{\mathrm{WT,min}} + \Delta\epsilon_{\mathrm{WT}}, \\ & \epsilon_{\mathrm{load},i} = \epsilon_{\mathrm{load,min}} + \Delta\epsilon_{\mathrm{load}}, \\ & C \le (1+\delta)\, C_0, \\ & \text{s.t.}(9)\text{–}(21),\ (26)\text{–}(31),\ (35)\text{–}(36),\ (39)\text{–}(54),\ (59),\ (65)\text{–}(67), \end{aligned} \tag{69}$$

where $\epsilon_{\mathrm{WT,max}}$ and $\epsilon_{\mathrm{WT,min}}$ are the maximum and minimum values under the sole action of α_{WT}, respectively. $\epsilon_{\mathrm{WT},i}$ is the ith threshold value of α_{WT}. $\Delta\epsilon_{\mathrm{WT}} = (\epsilon_{\mathrm{WT,max}} - \epsilon_{\mathrm{WT,min}})i/g$. $\Delta\epsilon_{\mathrm{load}} = (\epsilon_{\mathrm{load,max}} - \epsilon_{\mathrm{load,min}})i/g$. g is the number of equally spaced grid points. $i = 1, \cdots, g$.

The compromised solution is selected using fuzzy decision making [97]. In fuzzy decision making, the membership value μ_i^j for ith objective of jth solution on the Pareto front is given by the membership function:

$$\mu_i^j = \begin{cases} 1 & \text{if } f_i \ge f_i^{\max} \\ \frac{f_i - f_i^{\min}}{f_i^{\max} - f_i^{\min}} & \text{if } f_i^{\min} \le f_i < f_i^{\max} \\ 0 & \text{if } f_i < f_i^{\min} \end{cases}, \tag{70}$$

where $f_i^{\max}$ and $f_i^{\min}$ are the maximum and minimum values of solutions on the Pareto front.

The normalized membership value of the jth solution is governed by

$$\mu^j = \frac{\sum_{i=1}^{M} \mu_i^j}{\sum_{j=1}^{K}\sum_{i=1}^{M} \mu_i^j}, \tag{71}$$

where K indicates the number of Pareto solutions, and M represents the number of multiple objectives. The Pareto solution which has the maximum value of μ^j is selected as the best solution.

5.4.2. OM

Constraints (60)–(62) in OM can be converted to

$$P_{j,t}^{\mathrm{WT}} = (1+\alpha_{\mathrm{WT}})\tilde{P}_{j,t}^{\mathrm{WT}}, \tag{72}$$

$$P_{j,t}^{\mathrm{PV}} = (1+\alpha_{\mathrm{PV}})\tilde{P}_{j,t}^{\mathrm{PV}}, \tag{73}$$

$$P_{j,t}^{\mathrm{load}} = (1-\alpha_{\mathrm{load}})\tilde{P}_{j,t}^{\mathrm{load}}. \tag{74}$$

Problem (64) is a multi-objective bi-level problem; similarly, it can be transformed into the following problem:

$$\begin{aligned} \min \quad & \alpha_{\mathrm{PV}} \\ \text{s.t.} \quad & \alpha_{\mathrm{WT}} \le \epsilon_{\mathrm{WT},i} \\ & \alpha_{\mathrm{load}} \le \epsilon_{\mathrm{load},i}, \\ & \epsilon_{\mathrm{WT},i} = \epsilon_{\mathrm{WT,min}} + \Delta i_{\mathrm{WT}}, \\ & \epsilon_{\mathrm{load},i} = \epsilon_{\mathrm{load,min}} + \Delta i_{\mathrm{load}}, \\ & C \le (1-\kappa)\, C_0, \\ & (9)\text{–}(21),\ (26)\text{–}(31),\ (35)\text{–}(36),\ (39)\text{–}(54),\ (59),\ (72)\text{–}(74). \end{aligned} \tag{75}$$

By changing (70) slightly, we obtain the membership function for OM.

5.5. Model solving method

After the model conversion as delineated in Section 5.4, the multi-objective bi-level programming problems are finally transformed into the MILP problems, which can be solved by off-the-shelf commercial softwares such as GUROBI. The comprehensive solution process of multi-objective models for optimal microgrid planning and operation based on info-gap theory is illustrated in Figure 7. As can be seen from Figure 7, the solution process is divided into two stages. The results of the first stage are obtained by Algorithm 4, and at the first stage, it is considered that the predicted values of the uncertain parameters are perfect and completely accurate. The results of the second stage are obtained by Algorithm 5.

Algorithm 4 Algorithm for deterministic microgrid planning and operation model

Input: Predicted data of renewables and loads, parameters of DERs, price and other economic data, time horizon, time resolution, topology and relevant data of the microgrid.

Output: Base cost C_0

1: Generate typical scenarios based on WGAN-GP and K-medoids.
2: Calculate the actual BESS lifetime based on the rain-flow counting algorithm.
3: Solve the deterministic microgrid planning and operation model, i.e., Problem (55).
4: Obtain the base cost.

6. Case studies

6.1. Test platform and case description

The proposed models are tested on Feeder 1 of the Banshee microgrid [98], as shown in Figure 8. Bus 1 is the PCC. The loads at Buses 2–5 are interruptible, the loads at Buses 4–6 are critical, and the loads at Bus 7 are priority. The peak loads of Buses 1–7 are 0, 0.3, 0, 1.2, 0.25, 1.5, and 1 MVA, respectively. Based on the original data in [99, 100], the wind, PV generation, and load scenarios of 36 typical days used in this paper are generated using WGAN-GP and K-medoids techniques described in Sections 2.1 and 2.2. The time resolution is one hour. The total number of optimization hours throughout the year is $36 \times 24 = 864$,

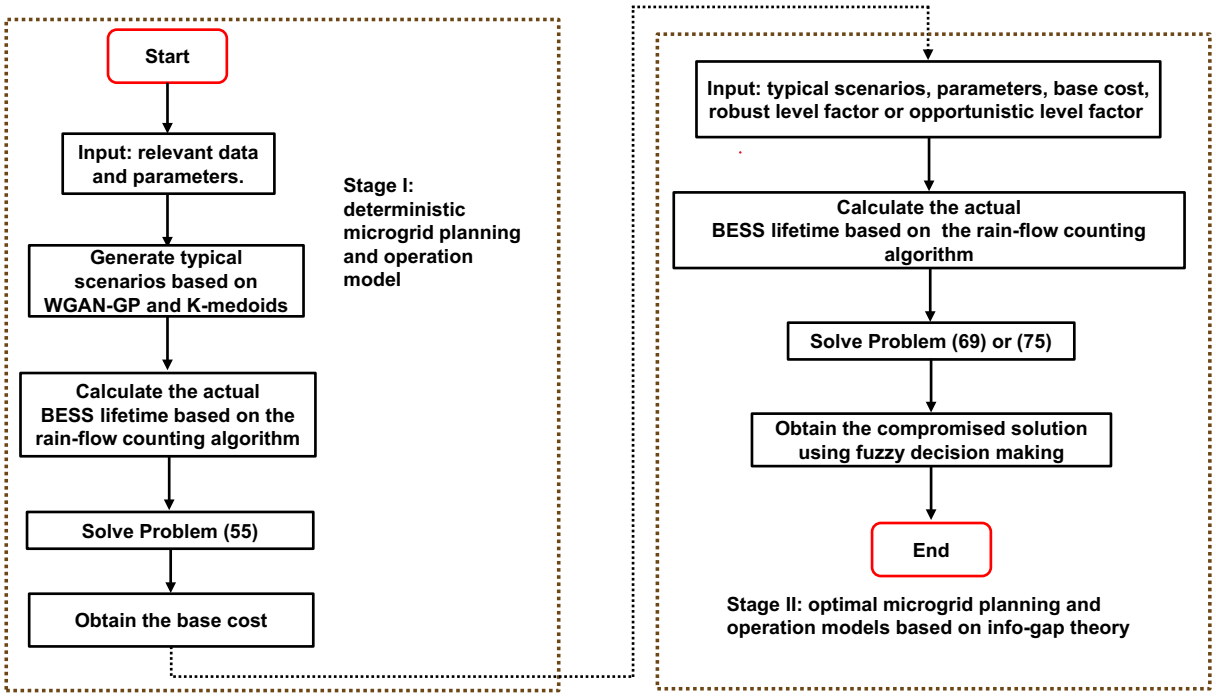

Figure 7: Flowchart of solving multi-objective models for optimal microgrid planning and operation based on info-gap theory.

Algorithm 5 Algorithm for optimal microgrid planning and operation models based on info-gap theory

Input: Typical scenarios, base cost, parameters of DERs, price and other economic data, time horizon, time resolution, topology and relevant data of the microgrid, robust level factor or opportunistic level factor.

Output: Optimal DER installation capacity, type, location, microgrid operation data, investment cost, operation cost, total cost, horizons of the uncertainties of wind, PV generation, and loads, α_{WT}, α_{PV}, and α_{load}.

1: Calculate the actual BESS lifetime based on the rain-flow counting algorithm.
2: Solve the RM model, i.e., Problem (69), or the OM model, i.e., Problem (75).
3: Obtain the compromised solution using fuzzy decision making.

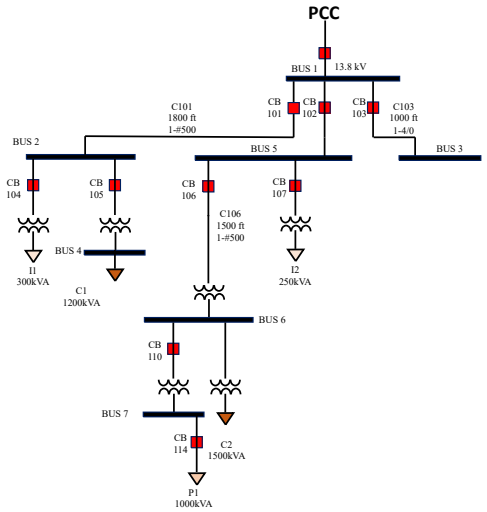

Figure 8: Feeder 1 of the Banshee microgrid.

which is much less than the number of annual 8760 hours and make the calculation tractability and calculation efficiency greatly improved.

The parameters of DERs are shown in Table 3. The import, export rate, and curtailment cost are \$0.15/kWh, \$0.09/kWh, and \$0.18/kWh, respectively [1, 101]. The minimum and maximum acceptable voltage magnitude thresholds are $|\underline{V}| = 0.9\,\text{p.u.}$ and $|\overline{V}| = 1.05\,\text{p.u.}$, respectively. For BESSs, $\delta = 0.01\,\%/\text{h}$; charging and discharging efficiency are both 95%. The planning horizon T is 15 years. The nominal discount rate i and the expected inflation rate f are 6.75% and 4.1%, respectively. The power factor pf is set to be 0.95 (lagging) [102, 103, 104, 105]. The emission characteristics of generation technologies and the magnitude of penalty for pollutant emissions are shown in Tables 4 [106].

Simulations are carried out on the desktop with an Intel i9 CPU, 3.60 GHz (16 CPUs), a 64 GB RAM, an Intel(R) UHD Graphics 630 GPU, and an NVIDIA GeForce RTX 2080 Ti GPU. Instead of closed source MATLAB, we use free and open source PYTHON. The solver is GUROBI.

Table 3: Parameters of DERs

Type of Cost	DG	BESS	PV	WT
Capital[1]	800	250	1875	900
OM[1]	35	10	22	22
Generation (\$/kWh)	0.36	/	/	/
Fixed Installation (\$)	1000	1000	1000	1000

[1] The units of capital and OM costs for BESSs and other DERs are \$/kWh and \$/kW, respectively.

Table 4: Emission characteristics of DEs and the magnitude of penalty for pollutant emissions

Pollutant Type	Emission characteristics (g/kWh)	Magnitude of penalty (\$/kg)
NO_x	4.3314	0.250
CO_2	232.0373	0.00125
CO	2.3204	0.020
SO_2	0.4641	0.125

6.2. Deterministic planning results

Supposing that the predicted value equals the actual value, we obtain C_0 and other planning results, as shown in Table 5. After obtaining wind, PV generation, and load scenarios of typical days, we solve Problem (55) to get the optimal solutions of all variables, which include the voltage amplitude of each bus. Then, we can obtain the voltage profiles of all buses on all typical days for deterministic planning as shown in Figure 9.

Table 5: Deterministic planning results

Type	Capacity[1]	Placement	Investment Cost (k\$)	Operation Cost (k\$)	Total Cost (k\$)
DG	2000	2	1238.52	1321.12	2559.64
WT	0	/			
BESS	2768	6			
PV	5468	6			

[1] The units of capacity for BESSs and other DERs are kWh and kW, respectively.

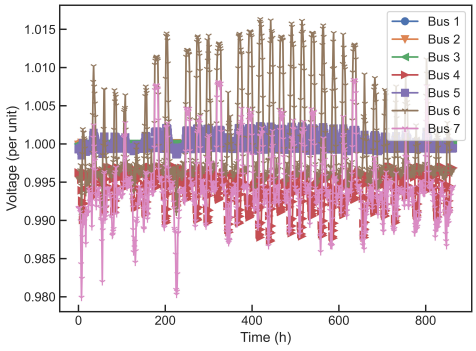

Figure 9: Voltage profiles of all buses on all typical days for deterministic planning.

6.3. Planning results based on the RM with RA

According to (69), we get the planning results based on the RM with RA, as shown in Table 6. Take $\delta = 0.20$ as an example; when wind, PV generation, and loads fluctuate at $[0.0099, 1.9901]\tilde{P}^{\mathrm{WT}}_{j,t}$, $[0.0108, 1.9892]\tilde{P}^{\mathrm{PV}}_{j,t}$, and $[0.8437, 1.1563]\tilde{P}^{\mathrm{load}}_{j,t}$, respectively, the planning cost of the microgrid does not exceed \$3071.56k. From the sensitivity analyses, as shown in Figure 10, we know that in the RM, both costs and the sum of uncertainty horizons are positively correlated with robust level factors. This is because the robust level factor represents the percentage of cost increases that planners can accept due to uncertainties. Generally, the larger robust level factor, the larger the budget of the planning scheme that the planner can bear, and the stronger the ability of the planning model to cope with uncertainties. Conservative decision makers believe that uncertainties will lead to the development of goals in an unfavorable direction and hope to make the system bear the maximum possible uncertainties by paying more planning costs.

When δ is equal to 0.20, 0.25, 0.30, and 0.35, respectively, the Pareto-optimal fronts of Problem (69) are shown in Figures 11–14, respectively. After obtaining wind, PV generation, and load scenarios of typical days, we solve Problem (69) to get the optimal solutions of all variables, which include the voltage amplitude of each bus. Then, we can obtain the voltage profiles of all buses on all typical days for the RM with RA when δ is equal to 0.20, 0.25, 0.30, and 0.35, respectively, which are shown in Figures 11–14. As can be seen from these figures, voltages are within the required range with high quality.

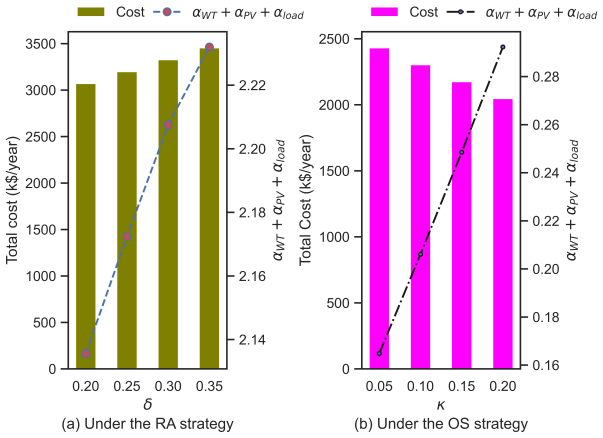

Figure 10: Variation trends of costs and uncertainties with level factors.

6.4. Planning results based on the OM with OS

According to (75), we get the planning results based on the OM with OS, as shown in Table 7. Likewise, take $\kappa = 0.05$ as an example; when the radii of the uncertainties of wind,

Table 6: Planning results based on the RM with RA

Type	Cap.	Pl.	δ	α_{WT}	α_{PV}	α_{load}	Investment Cost (k$)	Operation Cost (k$)	Total Cost (k$)
DG	2000	3							
WT	0	/							
BESS	5718	6	0.20	0.9901	0.9892	0.1563	1516.41	1555.15	3071.56
PV	1084×6	2–7							
DG	2000	3							
WT	0	/							
BESS	6294	3	0.25	0.9901	0.9889	0.1934	1561.59	1637.96	3199.55
PV	1110×6	2–7							
DG	2000	7							
WT	0	/							
BESS	7348	3	0.30	0.9901	0.9878	0.2296	1716.03	1611.50	3327.53
PV	1222×4,1250,1222	2–7							
DG	2000	6							
WT	0	/							
BESS	9259	4	0.35	0.9901	0.9859	0.2560	1981.16	1474.35	3455.51
PV	1411×2, 1486, 1411×3	2–7							

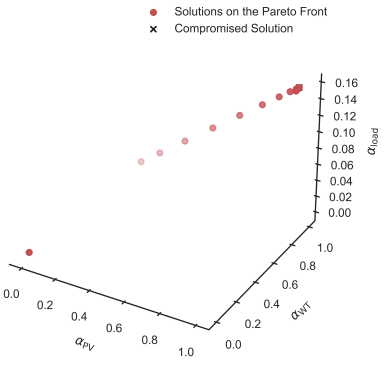

Figure 11: Pareto-optimal front of (69) when δ=0.20

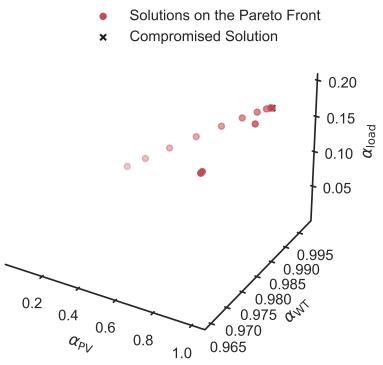

Figure 12: Pareto-optimal front of (69) when δ=0.25

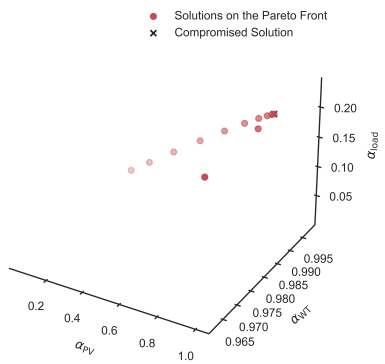

Figure 13: Pareto-optimal front of (69) when δ=0.30

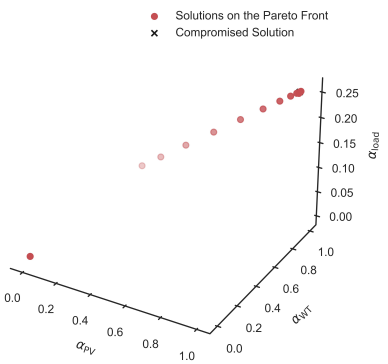

Figure 14: Pareto-optimal front of (69) when δ=0.35

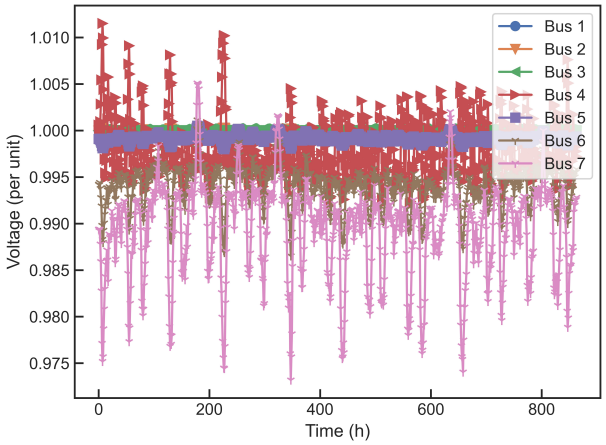

Figure 15: Voltage profiles under RM when $\delta = 0.20$

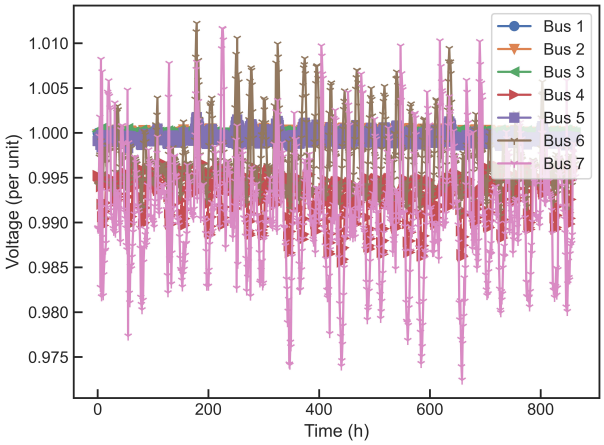

Figure 16: Voltage profiles under RM when $\delta = 0.25$

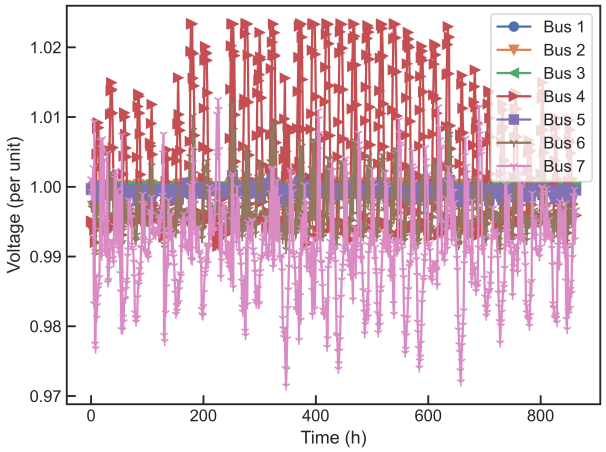

Figure 17: Voltage profiles under RM when $\delta = 0.30$

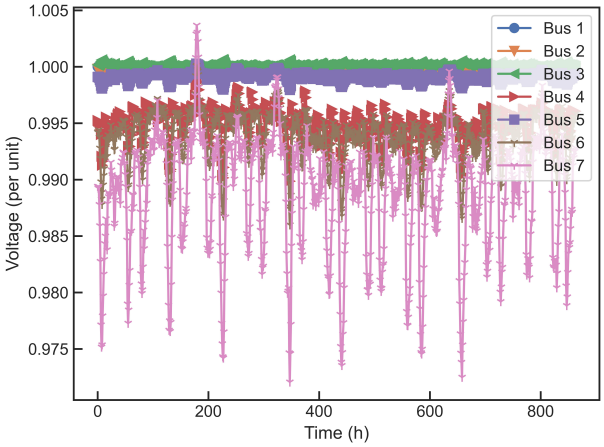

Figure 18: Voltage profiles under RM when $\delta = 0.35$

PV generation, and loads are 0.0625, 0, and 0.1023, respectively, the planning cost of the microgrid does not exceed \$2431.65k. From the sensitivity analyses, as shown in Figure 10, we know that in the OM, costs are negatively correlated with opportunistic level factors, while the sum of uncertainty horizons is positively correlated with the opportunistic level factor. This is because OS decision makers believe that uncertainties will lead to a favorable development of the problem, and they are more inclined to accept lower planning costs. After obtaining wind, PV generation, and load scenarios of typical days, we solve Problem (75) to get the optimal solutions of all variables, which include the voltage amplitude of each bus. Then, we can obtain the voltage profiles of all buses on all typical days for the OM with OS when κ is equal to 0.05, 0.10, 0.15, and 0.20, respectively, which are shown in Figures 19–22. As can be seen from these figures, the voltages fully meet the requirements with high quality.

Table 7: Planning results based on the OM with OS

Type	Cap.	Pl.	κ	α_{WT}	α_{PV}	α_{load}	Investment Cost (k\$)	Operation Cost (k\$)	Total Cost (k\$)
DG	2000	7	0.05	0.0625	0	0.1023	679.14	1752.51	2431.65
WT	0	/							
BESS	0	/							
PV	2757	6							
DG	2000	7	0.10	0.0625	0	0.1436	637.09	1666.58	2303.67
WT	0	/							
BESS	0	/							
PV	2514	7							
DG	2000	7	0.15	0.0625	0	0.1860	608.38	1567.31	2175.69
WT	0	/							
BESS	0	/							
PV	2348	7							
DG	2000	7	0.20	0.0625	0	0.2298	579.48	1468.23	2047.71
WT	0	/							
BESS	0	/							
PV	2181	7							

6.5. Verification by the Monte Carlo method

In order to further verify the models presented in this paper, 100 Monte Carlo simulation experiments were conducted in uncertain scenarios. Take the RA strategy as an example. According to the distribution of the costs under RM shown in Figure 23 and the kernel density estimate plot under RM shown in Figure 24, when $\delta = 0.25$ and wind, PV generation, and loads fluctuate within $[0.0099, 1.9901]\tilde{P}^{\text{WT}}_{j,t}$, $[0.0111, 1.9889]\tilde{P}^{\text{PV}}_{j,t}$, and $[0.8066, 1.1934]\tilde{P}^{\text{load}}_{j,t}$, respectively, the planning model under the RA strategy guarantees that the planning cost is not greater than the expected value $2559.64\text{k} \times (1 + 0.25) = \$3199.55\text{k}$. The experimental results show that the planning model under the multi-objective RA strategy can ensure that the planning cost is not greater than the expected cost, which verifies the feasibility and effectiveness of the models proposed in this paper.

6.6. Influence of power factors on results

When the power factor is 0.90 and 0.85, respectively, we are able to get the results for the different models as shown in Tables 8–10. As can be seen from Tables 8–10, for the deterministic model, when the power factor decreases, the total cost increases, and the installation capacities of some DERs change. For the RM model, when the robust level factor is certain, the total cost increases with the decrease of the power factor. As the power factor changes, both the

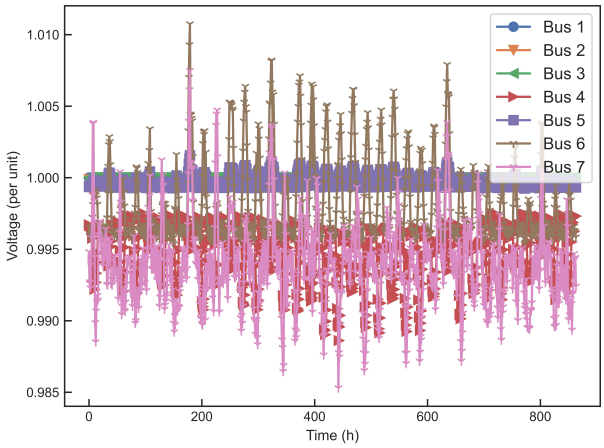

Figure 19: Voltage profiles under OM when $\kappa = 0.05$

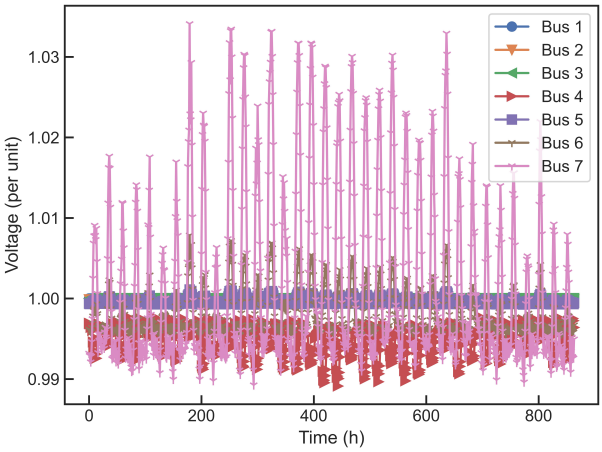

Figure 20: Voltage profiles under OM when $\kappa = 0.10$

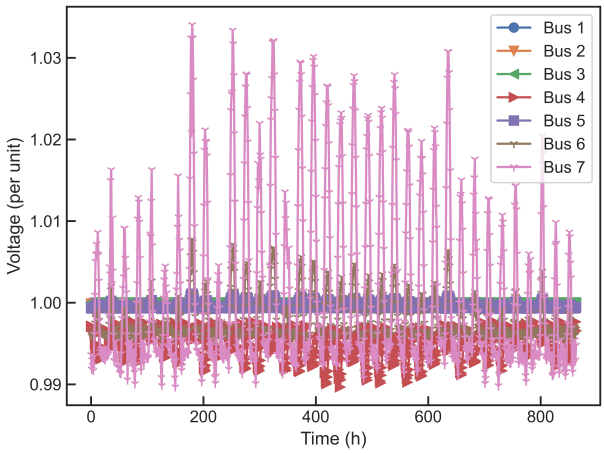

Figure 21: Voltage profiles under OM when $\kappa = 0.15$

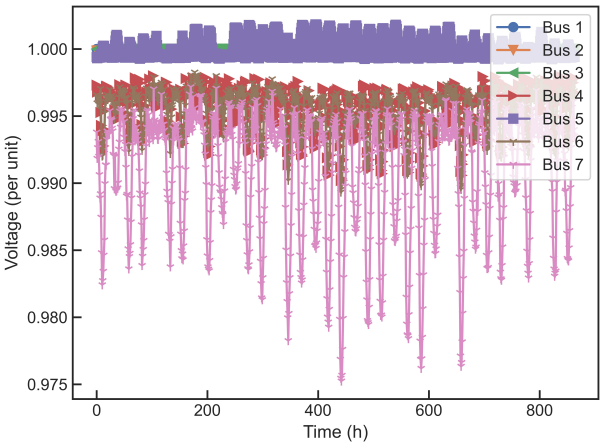

Figure 22: Voltage profiles under OM when $\kappa = 0.20$

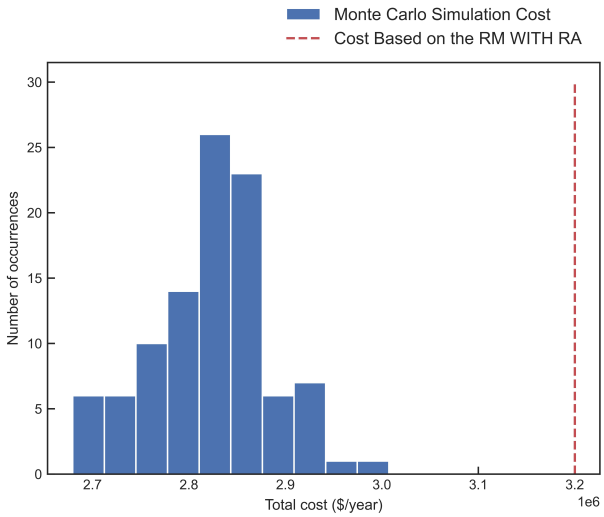

Figure 23: Distribution of the costs under RM.

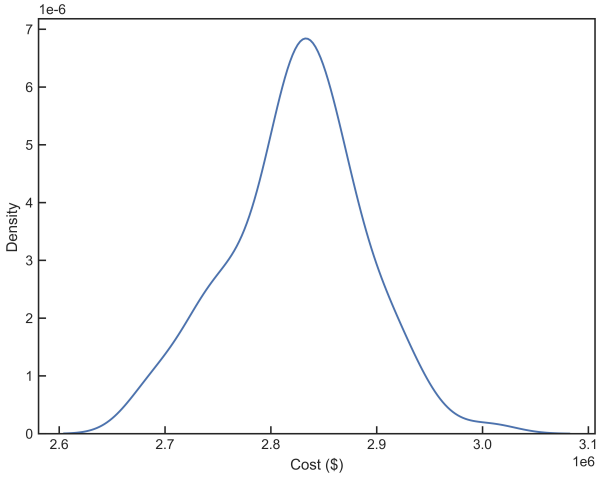

Figure 24: Density of the costs under RM.

installation capacities and placement of some DERs change. With the reduction of the power factor, the sum of uncertainty horizons may not change or may become larger. For the OM model, when the opportunistic level factor is certain, the total cost increases with the decrease of the power factor. Similarly, both the installation capacities and placement of some DERs change with the change of the power factor. With the reduction of the power factor, the sum of uncertainty horizons may not change or may become smaller.

Table 8: Deterministic planning results when the power factor is 0.90 and 0.85, respectively

Type	Capacity	Placement	pf	Investment Cost (k$)	Operation Cost (k$)	Total Cost (k$)
DG	2000	2	0.90	1238.83	1320.88	2559.70
WT	0	/				
BESS	2785	6				
PV	5467	6				
DG	2000	2	0.85	1237.78	1322.32	2560.11
WT	0	/				
BESS	2864	6				
PV	5447	6				

Table 9: Planning results based on the RM with RA when the power factor is 0.90 and 0.85, respectively

Type	Cap.	Pl.	pf	δ	α_{WT}	α_{PV}	α_{load}	Investment Cost (k$)	Operation Cost (k$)	Total Cost (k$)
DG	2000	7	0.90	0.25	0.9901	0.9889	0.1934	1560.24	1639.39	3199.63
WT	0	/								
BESS	6277	4								
PV	1109×6	2–7								
DG	2000	3	0.85	0.25	0.9969	0.9827	0.1949	1617.87	1582.27	3200.13
WT	0	/								
BESS	6713	2								
PV	1730×2, 1730×2	2–3, 5–6								

Table 10: Planning results based on the OM with OS when the power factor is 0.90 and 0.85, respectively

Type	Cap.	Pl.	pf	κ	α_{WT}	α_{PV}	α_{load}	Investment Cost (k$)	Operation Cost (k$)	Total Cost (k$)
DG	2000	7	0.90	0.10	0.0625	0	0.1436	638.87	1664.87	2303.73
WT	0	/								
BESS	0	/								
PV	2524	7								
DG	2000	7	0.85	0.10	0.0625	0	0.1435	673.72	1630.38	2304.10
WT	0	/								
BESS	0	/								
PV	2726	6								

7. Conclusion

In view of the shortcomings of GANs and WGANs, such as difficult training, slow convergence rate, and poor sample quality, this paper applies WGAN-GP to wind, PV generation, and load scenario generation, and utilizes the K-medoids reduction technology to obtain several

typical scenarios to reduce the calculation burden. The performance of WGAP-GP is better than that of WGANs, the training of WGAP-GP is stable, and almost no parameters are needed to tune. This paper considers the actual lifetime of the BESS based on the rain-flow counting algorithm, so as to consider the replacement cost of the BESS. We derive an MILP model for the deterministic planning and operation of the microgrid in a strict mathematical way. This MILP model takes into account dynamic constraints such as power flow and system reserve constraints, BESS replacement, and other equipment replacement costs in the objective function, which are not considered in many references. Based on info-gap theory, this paper comprehensively considers the uncertainties of wind, PV generation, and loads, and establishes two multi-objective bi-level planning models with robustness and opportunity respectively according to the difference in attitude to risk. All models proposed in this paper are multi-bus models, which can not only give the total capacity of DERs, but also the placement of DERs. Finally, these models are transformed into multi-objective single level programming and solved by the ϵ-constraint method. The following results are obtained through the analyses of case studies.

1) In the RM, both costs and the sum of uncertainty horizons are positively correlated with robust level factors. In the OM, costs are negatively correlated with opportunistic level factors; however, the sum of uncertainty horizons is positively correlated with the opportunistic level factor.

2) The RM model can effectively deal with the negative effects of uncertainty and guarantee certain expected costs while realizing the robustness of the system; however, the OM model can make full use of favorable uncertainties and obtain lower expected costs.

3) The Monte Caro simulation results also demonstrate that the RM model can ensure that the planning cost is not greater than the expected cost, which verifies the feasibility and effectiveness of the models proposed in this paper.

4) For the deterministic model, as the power factor decreases, the total cost increases. For the RM model or the OM model, when the robust level factor or the opportunistic level factor is certain, the total cost increases with the decrease of the power factor. For the RM model, the sum of uncertainty horizons may not change or may become larger with the reduction of the power factor. However, for the OM model, the sum of uncertainty horizons may not change or may become smaller with the reduction of the power factor. For the deterministic model, with the change of the power factor, the installation capacities of some DERs change. For the RM model and the OM model, with the change of the power factor, both the capacities and placement of some DERs change.

5) The ϵ-constraint method can efficiently solve the multi-objective optimization problems in this paper.

6) For uncertainty modeling, info-gap theory has the advantages of less required information and no need for probability distribution information. However, uncertainty modeling with info-gap theory also has some weaknesses, such as choosing the robust model or the opportunity model in practical engineering, and how to determine appropriate robust level factors or appropriate opportunistic level factors, all of which require experience.

In our future research, we will focus on the following directions.

1) We will study the optimal configurations of flywheel energy storage, compressed air energy storage, supercapacitor energy storage, superconducting energy storage, and lead-acid battery energy storage in microgrid planning based on info-gap theory and compare their

economy. We will also study the optimal configurations of hybrid energy storage in microgrid planning based on info-gap theory, such as battery-supercapacitor hybrid energy storage, and compare their economy.

2) We will study the optimal planning and operation of integrated energy systems based on info-gap theory. We will consider more uncertainties, such as market price fluctuations, policy changes, and technological advancements, and explore their impact on the planning and operation of microgrids and integrated energy systems. We will consider electric vehicles, hydrogen vehicles, and other new loads as well. We will also take into account different demand-side responses in the models. Considering so many factors can make modeling very complex. Solving these models will be very challenging. How to efficiently solve these complex models is a problem well worth studying.

3) We intend to compare different models based on info-gap theory, stochastic programming, robust optimization, and interval optimization from the performance of uncertainty modeling, such as modeling accuracy, costs, and computational complexity. We will also explore the combination of various uncertainty modelling methods in order to obtain better hybrid methods for uncertainty modelling. Solving these hybrid models can be a tricky problem.

4) We will explore applying exact power flow equations to our models and compare models based on exact power flow with models based on LinDistFlow. The models considering the exact power flow are highly non-convex nonlinear models, and the solution of the models will be complex and time-consuming.

5) We will include more objectives, such as low carbon requirements, to form many-objective models, and will study how to design more efficient multi-objective and many-objective solution methods. Generally speaking, the speed of the classical multi-objective algorithm is faster than that of the heuristic algorithm, but the classical algorithm has high requirements for the properties of the model itself. Exploring the combination of heuristic algorithms and classical algorithms is an interesting and important topic, but also a knotty one.

References

[1] X. Cao, J. Wang, B. Zeng, A chance constrained information-gap decision model for multi-period microgrid planning, IEEE Transactions on Power Systems 33 (3) (2017) 2684–2695.

[2] M. Rahmani-Andebili, Applications of Fuzzy Logic in Planning and Operation of Smart Grids, Springer, 2021.

[3] Y. Mohammadi, H. Shakouri, A. Kazemi, A multi-objective fuzzy optimization model for electricity generation and consumption management in a micro smart grid, Sustainable Cities and Society 86 (2022) 104119.

[4] R. Morales, D. Sáez, L. G. Marin, A. Nunez, Microgrid planning based on fuzzy interval models of renewable resources, in: 2016 IEEE International Conference on Fuzzy Systems (FUZZ-IEEE), IEEE, 2016, pp. 336–343.

[5] V. Miranda, P. S. Hang, Economic dispatch model with fuzzy wind constraints and attitudes of dispatchers, IEEE Transactions on power systems 20 (4) (2005) 2143–2145.

[6] R.-H. Liang, J.-H. Liao, A fuzzy-optimization approach for generation scheduling with wind and solar energy systems, IEEE transactions on power systems 22 (4) (2007) 1665–1674.

[7] M. Banaei, B. Rezaee, Fuzzy scheduling of a non-isolated micro-grid with renewable resources, Renewable Energy 123 (2018) 67–78.

[8] Y. Zhang, F. Meng, R. Wang, W. Zhu, X.-J. Zeng, A stochastic mpc based approach to integrated energy management in microgrids, Sustainable cities and society 41 (2018) 349–362.

[9] Z. Li, X. Xie, Z. Cheng, C. Zhi, J. Si, A novel two-stage energy management of hybrid AC/DC microgrid considering frequency security constraints, International Journal of Electrical Power & Energy Systems 146 (2023) 108768.

[10] H. Kim, M. Kim, J. Lee, A two-stage stochastic p-robust optimal energy trading management in microgrid operation considering uncertainty with hybrid demand response, International Journal of Electrical Power & Energy Systems 124 (2021) 106422.

[11] G. Martinez, N. Gatsis, G. B. Giannakis, Stochastic programming for energy planning in microgrids with renewables, in: 2013 5th IEEE International Workshop on Computational Advances in Multi-Sensor Adaptive Processing (CAMSAP), IEEE, 2013, pp. 472–475.

[12] M. Shaterabadi, M. A. Jirdehi, Multi-objective stochastic programming energy management for integrated invelox turbines in microgrids: A new type of turbines, Renewable Energy 145 (2020) 2754–2769.

[13] D. Han, J. H. Lee, Two-stage stochastic programming formulation for optimal design and operation of multi-microgrid system using data-based modeling of renewable energy sources, Applied Energy 291 (2021) 116830.

[14] Y. Cao, Y. Mu, H. Jia, X. Yu, K. Hou, H. Wang, A multi-objective stochastic optimization approach for planning a multi-energy microgrid considering unscheduled islanded operation, IEEE Transactions on Sustainable Energy (2023).

[15] H. Farzin, M. Fotuhi-Firuzabad, M. Moeini-Aghtaie, A stochastic multi-objective framework for optimal scheduling of energy storage systems in microgrids, IEEE Transactions on Smart Grid 8 (1) (2016) 117–127.

[16] S. F. Zandrazavi, C. P. Guzman, A. T. Pozos, J. Quiros-Tortos, J. F. Franco, Stochastic multi-objective optimal energy management of grid-connected unbalanced microgrids with renewable energy generation and plug-in electric vehicles, Energy 241 (2022) 122884.

[17] D. Yang, C. Jiang, G. Cai, D. Yang, X. Liu, Interval method based optimal planning of multi-energy microgrid with uncertain renewable generation and demand, Applied Energy 277 (2020) 115491.

[18] B. Wang, C. Zhang, Z. Y. Dong, Interval optimization based coordination of demand response and battery energy storage system considering soc management in a microgrid, IEEE Transactions on Sustainable Energy 11 (4) (2020) 2922–2931.

[19] Y. Li, P. Wang, H. B. Gooi, J. Ye, L. Wu, Multi-objective optimal dispatch of microgrid under uncertainties via interval optimization, IEEE Transactions on Smart Grid 10 (2) (2017) 2046–2058.

[20] C. Mu, Y. Shi, N. Xu, X. Wang, Z. Tang, H. Jia, H. Geng, Multi-objective interval optimization dispatch of microgrid via deep reinforcement learning, IEEE Transactions on Smart Grid (2023).

[21] Y. Jiang, C. Wan, C. Chen, M. Shahidehpour, Y. Song, A hybrid stochastic-interval operation strategy for multi-energy microgrids, IEEE Transactions on Smart Grid 11 (1) (2019) 440–456.

[22] M. Tostado Véliz, H. M. Hasanien, A. R. Jordehi, R. A. Turky, M. Gómez-González, F. Jurado, An interval-based privacy–aware optimization framework for electricity price setting in isolated microgrid clusters, Applied Energy 340 (2023) 121041.

[23] M. H. S. Boloukat, A. A. Foroud, Stochastic-based resource expansion planning for a grid-connected microgrid using interval linear programming, Energy 113 (2016) 776–787.

[24] X. Dai, Y. Li, K. Zhang, W. Feng, A robust offering strategy for wind producers considering uncertainties of demand response and wind power, Applied Energy 279 (2020) 115742.

[25] S. M. Hosseini, R. Carli, M. Dotoli, Robust optimal energy management of a residential microgrid under uncertainties on demand and renewable power generation, IEEE Transactions on Automation Science and Engineering 18 (2) (2020) 618–637.

[26] N. Amjady, A. Attarha, S. Dehghan, A. J. Conejo, Adaptive robust expansion planning for a distribution network with ders, IEEE Transactions on Power Systems 33 (2) (2017) 1698–1715.

[27] Y. Xiang, J. Liu, Y. Liu, Robust energy management of microgrid with uncertain renewable generation and load, IEEE Transactions on Smart Grid 7 (2) (2015) 1034–1043.

[28] Y. Yang, W. Wu, A distributionally robust optimization model for real-time power dispatch in distribution networks, IEEE Transactions on Smart Grid 10 (4) (2018) 3743–3752.

[29] Z. Yang, A. Trivedi, H. Liu, M. Ni, D. Srinivasan, Two-stage robust optimization strategy for spatially-temporally correlated data centers with data-driven uncertainty sets, Electric Power Systems Research 221 (2023) 109443.

[30] B. Zhao, J. Ren, J. Chen, D. Lin, R. Qin, Tri-level robust planning-operation co-optimization of distributed energy storage in distribution networks with high pv penetration, Applied Energy 279 (2020) 115768.

[31] K. Qu, T. Yu, Z. Pan, X. Zhang, Point estimate-based stochastic robust dispatch for electricity-gas combined system under wind uncertainty using iterative convex optimization, Energy 211 (2020) 118986.

[32] Y. Ben-Haim, Info-gap decision theory: decisions under severe uncertainty, Elsevier, 2006.

[33] A. K. Basu, A. Bhattacharya, S. Chowdhury, S. Chowdhury, Planned scheduling for economic power sharing in a CHP-based micro-grid, IEEE Transactions on Power systems 27 (1) (2011) 30–38.

[34] S. Bahramirad, W. Reder, A. Khodaei, Reliability-constrained optimal sizing of energy storage system in a microgrid, IEEE Transactions on Smart Grid 3 (4) (2012) 2056–2062.

[35] B. Yan, P. B. Luh, G. Warner, P. Zhang, Operation and design optimization of microgrids with renewables, IEEE Transactions on automation science and engineering 14 (2) (2017) 573–585.

[36] M. H. Moradi, M. Eskandari, S. M. Hosseinian, Operational strategy optimization in an optimal sized smart microgrid, IEEE Transactions on Smart Grid 6 (3) (2014) 1087–1095.

[37] S. M. Hakimi, S. Moghaddas-Tafreshi, Optimal planning of a smart microgrid including demand response and intermittent renewable energy resources, IEEE Transactions on Smart Grid 5 (6) (2014) 2889–2900.

[38] Y. Yan, C. Zhang, K. Li, Z. Wang, An integrated design for hybrid combined cooling, heating and power system with compressed air energy storage, Applied Energy 210 (2018) 1151–1166.

[39] M. F. Zia, E. Elbouchikhi, M. Benbouzid, Optimal operational planning of scalable DC microgrid with demand response, islanding, and battery degradation cost considerations, Applied energy 237 (2019) 695–707.

[40] H. Lotfi, A. Khodaei, AC versus DC microgrid planning, IEEE Transactions on Smart Grid 8 (1) (2015) 296–304.

[41] S. X. Chen, H. B. Gooi, M. Wang, Sizing of energy storage for microgrids, IEEE transactions on smart grid 3 (1) (2011) 142–151.

[42] X. Wu, W. Zhao, X. Wang, H. Li, An MILP-based planning model of a photovoltaic/diesel/battery stand-alone microgrid considering the reliability, IEEE Transactions on Smart Grid 12 (5) (2021) 3809–3818.

[43] S. Mashayekh, M. Stadler, G. Cardoso, M. Heleno, A mixed integer linear programming approach for optimal DER portfolio, sizing, and placement in multi-energy microgrids, Applied Energy 187 (2017) 154–168.

[44] J. Wang, Z. J. Zhai, Y. Jing, C. Zhang, Particle swarm optimization for redundant building cooling heating and power system, Applied Energy 87 (12) (2010) 3668–3679.

[45] M. Jayachandran, G. Ravi, Design and optimization of hybrid micro-grid system, Energy Procedia 117 (2017) 95–103.

[46] R. Dufo-López, J. L. Bernal-Agustín, Design and control strategies of PV-diesel systems using genetic algorithms, Solar energy 79 (1) (2005) 33–46.

[47] L. Guo, W. Liu, J. Cai, B. Hong, C. Wang, A two-stage optimal planning and design method for combined cooling, heat and power microgrid system, Energy Conversion and Management 74 (2013) 433–445.

[48] D. Wei, A. Chen, B. Sun, C. Zhang, Multi-objective optimal operation and energy coupling analysis of combined cooling and heating system, Energy 98 (2016) 296–307.

[49] F. A. Mohamed, H. N. Koivo, Microgrid online management and balancing using multiobjective optimization, in: 2007 IEEE Lausanne Power Tech, IEEE, 2007, pp. 639–644.

[50] F. A. Mohamed, H. N. Koivo, Online management of microgrid with battery storage using multiobjective optimization, in: 2007 International Conference on Power Engineering, Energy and Electrical Drives, IEEE, 2007, pp. 231–236.

[51] J. L. Bernal-Agustín, R. Dufo-López, Multi-objective design and control of hybrid systems minimizing costs and unmet load, Electric Power Systems Research 79 (1) (2009) 170–180.

[52] B. Zhao, Y. Shi, X. Dong, W. Luan, J. Bornemann, Short-term operation scheduling in renewable-powered microgrids: A duality-based approach, IEEE Transactions on sustainable energy 5 (1) (2013) 209–217.

[53] X. Wang, W. Huang, N. Tai, M. Shahidehpour, C. Li, Two-stage full-data processing for microgrid planning with high penetrations of renewable energy sources, IEEE Transactions on Sustainable Energy 12 (4) (2021) 2042–2052.

[54] A. A. Hamad, M. E. Nassar, E. F. El-Saadany, M. Salama, Optimal configuration of isolated hybrid AC/DC microgrids, IEEE Transactions on Smart Grid 10 (3) (2018) 2789–2798.

[55] J. Zhang, K.-J. Li, M. Wang, W.-J. Lee, H. Gao, C. Zhang, K. Li, A bi-level program for the planning of an islanded microgrid including CAES, IEEE Transactions on Industry Applications 52 (4) (2016) 2768–2777.

[56] U. Akram, M. Khalid, S. Shafiq, Optimal sizing of a wind/solar/battery hybrid grid-connected microgrid system, IET Renewable Power Generation 12 (1) (2018) 72–80.

[57] J. Gao, J. Chen, B. Qi, Y. Zhao, K. Peng, X. Zhang, A cost-effective two-stage optimization model for microgrid planning and scheduling with compressed air energy storage and preventive maintenance, International Journal of Electrical Power & Energy Systems 125 (2021) 106547.

[58] G. Liu, M. Starke, B. Xiao, X. Zhang, K. Tomsovic, Microgrid optimal scheduling with chance-constrained islanding capability, Electric Power Systems Research 145 (2017) 197–206.

[59] T. Niknam, R. Azizipanah-Abarghooee, M. R. Narimani, An efficient scenario-based stochastic programming framework for multi-objective optimal micro-grid operation, Applied Energy 99 (2012) 455–470.

[60] A. Narayan, K. Ponnambalam, Risk-averse stochastic programming approach for microgrid planning under uncertainty, Renewable energy 101 (2017) 399–408.

[61] E. Hajipour, M. Bozorg, M. Fotuhi-Firuzabad, Stochastic capacity expansion planning of remote microgrids with wind farms and energy storage, IEEE transactions on sustainable energy 6 (2) (2015) 491–498.

[62] Y. Liu, L. Guo, R. Hou, C. Wang, X. Wang, A hybrid stochastic/robust-based multi-period investment planning model for island microgrid, International Journal of Electrical Power & Energy Systems 130 (2021) 106998.

[63] Z. Wang, B. Chen, J. Wang, J. Kim, M. M. Begovic, Robust optimization based optimal dg placement in microgrids, IEEE Transactions on Smart Grid 5 (5) (2014) 2173–2182.

[64] T. Ding, S. Liu, W. Yuan, Z. Bie, B. Zeng, A two-stage robust reactive power optimization considering uncertain wind power integration in active distribution networks, IEEE Transactions on Sustainable Energy 7 (1) (2015) 301–311.

[65] L. Ji, D. Niu, G. Huang, An inexact two-stage stochastic robust programming for residential micro-grid management-based on random demand, Energy 67 (2014) 186–199.

[66] E. Samani, F. Aminifar, Tri-level robust investment planning of ders in distribution networks with ac constraints, IEEE Transactions on Power Systems 34 (5) (2019) 3749–3757.

[67] A. Khodaei, S. Bahramirad, M. Shahidehpour, Microgrid planning under uncertainty, IEEE Transactions on Power Systems 30 (5) (2014) 2417–2425.

[68] S. Nojavan, K. Zare, M. R. Feyzi, Optimal bidding strategy of generation station in power market using information gap decision theory (igdt), Electric Power Systems Research 96 (2013) 56–63.

[69] A. Mehdizadeh, N. Taghizadegan, J. Salehi, Risk-based energy management of renewable-based microgrid using information gap decision theory in the presence of peak load management, Applied energy 211 (2018) 617–630.

[70] A. H. Shojaei, A. A. Ghadimi, M. R. Miveh, F. H. Gandoman, A. Ahmadi, Multiobjective reactive power planning considering the uncertainties of wind farms and loads using information gap decision theory, Renewable Energy 163 (2021) 1427–1443.

[71] C. Murphy, A. Soroudi, A. Keane, Information gap decision theory-based congestion and voltage management in the presence of uncertain wind power, IEEE Transactions on Sustainable Energy 7 (2) (2015) 841–849.

[72] A. Rabiee, A. Soroudi, A. Keane, Information gap decision theory based OPF with HVDC connected wind farms, IEEE Transactions on Power Systems 30 (6) (2014) 3396–3406.

[73] A. Soroudi, A. Rabiee, A. Keane, Information gap decision theory approach to deal with wind power uncertainty in unit commitment, Electric Power Systems Research 145 (2017) 137–148.

[74] A. Ahmadi, A. E. Nezhad, P. Siano, B. Hredzak, S. Saha, Information-gap decision theory for robust security-constrained unit commitment of joint renewable energy and gridable vehicles, IEEE Transactions on Industrial Informatics 16 (5) (2019) 3064–3075.

[75] M. Ahrabi, M. Abedi, H. Nafisi, M. A. Mirzaei, B. Mohammadi-Ivatloo, M. Marzband, Evaluating the effect of electric vehicle parking lots in transmission-constrained ac unit commitment under a hybrid igdt-stochastic approach, International Journal of Electrical Power & Energy Systems 125 (2021) 106546.

[76] Y. Zhao, Z. Lin, F. Wen, Y. Ding, J. Hou, L. Yang, Risk-constrained day-ahead scheduling for concentrating solar power plants with demand response using info-gap theory, IEEE Transactions on Industrial Informatics 15 (10) (2019) 5475–5488.

[77] M. Moradi-Dalvand, B. Mohammadi-Ivatloo, N. Amjady, H. Zareipour, A. Mazhab-Jafari, Self-scheduling of a wind producer based on information gap decision theory, Energy 81 (2015) 588–600.

[78] J. C. Tinitana, C. Correa-Florez, D. Patino, J. Vuelvas, L. Aleaga, J. Carrión, Economic dispatch problem based on risk-seeking igdt approach, in: 2023 3rd International Conference on Electrical, Computer, Communications and Mechatronics Engineering (ICECCME), IEEE, 2023, pp. 1–6.

[79] A. M. Rostami, H. Ameli, M. T. Ameli, G. Strbac, Information-gap decision theory for robust operation of integrated electricity and natural gas transmission networks, in: 2020 International Conference on Smart Energy Systems and Technologies (SEST), IEEE, 2020, pp. 1–6.

[80] K. Vemalaiah, D. K. Khatod, N. P. Padhy, Optimal day-ahead scheduling of distributed energy resources: A strategy based on information gap decision theory to address multiple uncertainties in the active distribution networks, in: 2023 IEEE International Conference on Energy Technologies for Future Grids (ETFG), IEEE, 2023, pp. 1–6.

[81] B. Mohammadi-Ivatloo, H. Zareipour, N. Amjady, M. Ehsan, Application of information-gap decision theory to risk-constrained self-scheduling of gencos, IEEE Transactions on Power Systems 28 (2) (2012) 1093–1102.

[82] F. S. Gazijahani, J. Salehi, Igdt-based complementarity approach for dealing with strategic decision making of price-maker VPP considering demand flexibility, IEEE Transactions on Industrial Informatics 16 (4) (2019) 2212–2220.

[83] Q. Yan, H. Lin, J. Li, X. Ai, M. Shi, M. Zhang, D. Gejirifu, Many-objective charging optimization for electric vehicles considering demand response and multi-uncertainties based on markov chain and information gap decision theory, Sustainable Cities and Society 78 (2022) 103652.

[84] M. Salimi, M.-A. Nasr, S. H. Hosseinian, G. B. Gharehpetian, M. Shahidehpour, Information gap decision theory-based active distribution system planning for resilience enhancement, IEEE Transactions on Smart Grid 11 (5) (2020) 4390–4402.

[85] Y. Li, J. Wang, Y. Han, Q. Zhao, X. Fang, Z. Cao, Robust and opportunistic scheduling of district integrated natural gas and power system with high wind power penetration considering demand flexibility and compressed air energy storage, Journal of Cleaner Production 256 (2020) 120456.

[86] M. A. Mirzaei, A. Sadeghi-Yazdankhah, B. Mohammadi-Ivatloo, M. Marzband, M. Shafiekhah, J. P. Catalão, Integration of emerging resources in IGDT-based robust scheduling of combined power and natural gas systems considering flexible ramping products, Energy 189 (2019) 116195.

[87] L. Zuo, S. Wang, Y. Sun, S. Cui, J. Fang, X. Ai, B. Li, C. Hao, J. Wen, Robustness assessment of wind power generation considering rigorous security constraints for power system: A hybrid RLO-IGDT approach, CSEE Journal of Power and Energy Systems (2023).

[88] M. Arjovsky, S. Chintala, L. Bottou, Wasserstein generative adversarial networks, in: International conference on machine learning, PMLR, 2017, pp. 214–223.

[89] Y. Chen, Y. Wang, D. Kirschen, B. Zhang, Model-free renewable scenario generation using generative adversarial networks, IEEE Transactions on Power Systems 33 (3) (2018) 3265–3275.

[90] I. Gulrajani, F. Ahmed, M. Arjovsky, V. Dumoulin, A. C. Courville, Improved training of wasserstein gans, Advances in neural information processing systems 30 (2017).

[91] H. Heitsch, W. Römisch, Scenario reduction algorithms in stochastic programming, Computational optimization and applications 24 (2003) 187–206.

[92] N. Growe-Kuska, H. Heitsch, W. Romisch, Scenario reduction and scenario tree construction for power management problems, in: 2003 IEEE Bologna Power Tech Conference Proceedings,, Vol. 3, IEEE, 2003, pp. 7–pp.

[93] S. D. Downing, D. Socie, Simple rainflow counting algorithms, International journal of fatigue 4 (1) (1982) 31–40.

[94] E. Schaltz, A. Khaligh, P. O. Rasmussen, Influence of battery/ultracapacitor energy-storage sizing on battery lifetime in a fuel cell hybrid electric vehicle, IEEE Transactions on Vehicular Technology 58 (8) (2009) 3882–3891.

[95] V. I. Herrera, H. Gaztañaga, A. Milo, A. Saez-de Ibarra, I. Etxeberria-Otadui, T. Nieva, Optimal energy management of a battery-supercapacitor based light rail vehicle using genetic algorithms, in: 2015 IEEE Energy Conversion Congress and Exposition (ECCE), IEEE, 2015, pp. 1359–1366.

[96] M. E. Baran, F. F. Wu, Network reconfiguration in distribution systems for loss reduction and load balancing, IEEE Transactions on Power delivery 4 (2) (1989) 1401–1407.

[97] P. M. Pradhan, G. Panda, Pareto optimization of cognitive radio parameters using multiobjective evolutionary algorithms and fuzzy decision making, Swarm and Evolutionary Computation 7 (2012) 7–20.

[98] R. Salcedo, E. Corbett, C. Smith, E. Limpaecher, R. Rekha, J. Nowocin, G. Lauss, E. Fonkwe, M. Almeida, P. Gartner, et al., Banshee distribution network benchmark and prototyping platform for hardware-in-the-loop integration of microgrid and device controllers, The Journal of Engineering 2019 (8) (2019) 5365–5373.

[99] National Renewable Energy Laboratory (NREL), End-use load profiles for the U.S. building stock, available: https://data.openei.org/submissions/4520 (2021. [Online]).

[100] Office of Energy Efficiency & Renewable Energy, Commercial reference buildings, available: https://www.energy.gov/eere/buildings/commercial-reference-buildings (2011. [Online]).

[101] S. Meena, H. Liu, H. Tu, S. Lukic, W. Tang, A benchmarking tool for state-of-the-art microgrid design approache, in: 2023 Energy Conversion Conference & Expo (ECCE), IEEE, 2023, pp. 1–8.

[102] G. S. E. Solutions, Power factor and grid-connected photovoltaics, GSES Technical Papers, ed (2016).

[103] D. S. Sarma, L. Cupelli, F. Ponci, A. Monti, Distributed optimal power flow with data-driven sensitivity computation, in: 2021 IEEE Madrid PowerTech, IEEE, 2021, pp. 1–6.

[104] Y. Vilaisarn, AC microgrids analysis, optimization and planning for resilience enhancement, Ph.D. thesis, Université Laval (2022).

[105] R. Haider, Physics-aware optimization and data-driven methods for low-carbon power systems, Ph.D. thesis, Massachusetts Institute of Technology (2023).

[106] K. Qian, C. Zhou, Y. Yuan, X. Shi, M. Allan, Analysis of the environmental benefits of distributed generation, in: 2008 IEEE Power and Energy Society General Meeting-Conversion and Delivery of Electrical Energy in the 21st Century, IEEE, 2008, pp. 1–5.